Improving Model Calibrations in a Changing World: Controlling for Nonstationarity After Mega Disturbance Reduces Hydrological Uncertainty

Elijah N. Boardman^{1,2}, Gabrielle F. S. Boisramé³, Mark S. Wigmosta⁴, Robert K. Shriver⁵, Adrian A. Harpold^{1,5}

¹Graduate Program of Hydrologic Sciences, University of Nevada, Reno, Reno, Nevada, 89557, USA

Correspondence to: Elijah N. Boardman (eli.boardman@mountainhydrology.com)

Abstract. Model simulations are widely used to understand, predict, and respond to environmental changes, but uncertainty in these models can hinder decision-making. The simulation of hydrological changes after a forest fire is a typical example where process-based models with uncertain parameters may inform consequential predictions of water availability. Different parameter sets and meteorological forcing assumptions can yield similarly realistic simulations during model calibration but generate divergent predictions of change, a problem known as "equifinality." Despite longstanding recognition of the problems posed by equifinality, the implications for environmental disturbance simulations remain largely unconstrained. Here, we demonstrate how equifinality in water balance partitioning causes compounding uncertainty in hydrological changes attributable to a recent 1,540 km² megafire in the Sierra Nevada mountains (California, USA). Different model calibrations generate uncertain predictions of the four-year post-fire streamflow change that vary up to six-fold. However, controlling for nonstationary model error (e.g., a shift in the model bias after disturbance) can significantly (p < 0.01) reduce both equifinality and predictive uncertainty. Using a statistical metamodel to correct for bias shift after disturbance, we estimate a streamflow increase of 11% ±1% in the first four years after the fire, with an 18% ±4% increase during drought. Our metamodel framework for correcting nonstationarity reduces uncertainty in the post-fire streamflow change by 80% or 82% compared to the uncertainty of pure statistical or pure process-based model ensembles, respectively. As environmental disturbances continue to transform global landscapes, controlling for nonstationary biases can improve process-based models that are used to predict and respond to unprecedented hydrological changes.

²Mountain Hydrology LLC, Reno, Nevada, 89503, USA

³Hydrologic Sciences Division, Desert Research Institute, Reno, Nevada, 89512, USA

⁴Energy and Environment Directorate, Pacific Northwest National Laboratory, Richland, Washington, 99354, USA

⁵Department of Natural Resources and Environmental Science, University of Nevada, Reno, Reno, Nevada, 89557, USA

1 Introduction

particular watershed.

40

30 Calibration – systematic adjustment of model parameters to improve simulation accuracy.

Disturbance – an event that changes an environmental system from one state to another.

Equifinality – the production of similar results for different reasons.

Stationarity – the invariance of a statistical property across different time periods.

Environmental disturbances (e.g., forest fires, other vegetation mortality events, floods, anthropogenic land cover conversion, etc.) can alter the structure and function of ecohydrological systems (Zehe and Sivapalan 2009, Ebel and Mirus 2014, Buma 2015, Johnstone et al. 2016). Climate change and environmental disturbances introduce nonstationarity into the hydrological cycle, which is disrupting longstanding statistical approaches to water resource and risk management (Milly et al. 2008, 2015, Hirsch 2011, Salas et al. 2012, Yang et al. 2021).

Pure statistical methods (e.g., regression models lacking an explicit physical foundation) can sometimes detect streamflow changes attributable to environmental disturbance by comparing measurements to a stationary model, which represents a nodisturbance counterfactual. In this context, a "counterfactual" refers to a hypothetical scenario in which a particular disturbance did not happen, so comparing the actual post-disturbance behavior to the modeled counterfactual enables attribution of disturbance effects. Statistical change attribution is generally applied across many years and numerous sites (e.g., Goeking and Tarboton 2022a, Hampton and Basu 2022, Williams et al. 2022) or in careful paired watershed studies to overcome climate/weather variability (e.g., Bart 2016, Manning et al. 2022, Johnson and Alila 2023, Kang and Sharma 2024). However, in a single watershed with a short post-disturbance record, pure data-driven statistical approaches are inherently limited.

Crucially, many water management decisions (e.g., reservoir release schedules) are made on a per-watershed and per-year basis, so large-scale retrospective statistical assessments of disturbance effects may not provide actionable insights in any

Spatially distributed process-based hydrological models, and related land surface or Earth system models, are a widely accepted tool that can overcome some limitations of statistical disturbance attribution (Fatichi et al. 2016, Pongratz et al. 2018, Fisher and Koven 2020). Because interannual climate variability often obscures hydrological changes caused by disturbance, counterfactual model experiments using an undisturbed control are a cornerstone of ecohydrological disturbance attribution studies (e.g., Moreno et al. 2016, Saksa et al. 2017, Boisramé et al. 2019, Meili et al. 2024). Moreover, key process representations (e.g., flow routing and the snowpack energy balance) are expected to generalize beyond observed conditions, providing a basis for the prediction of hydrological responses to out-of-sample events including extreme storms (e.g., Huang and Swain 2022), decadal-scale climate change (e.g., Tague et al. 2009), and unprecedented "megafires" (e.g., Abolafia-Rosenzweig et al. 2024). In this context, a megafire is any wildfire in excess of 400 km² (Ayars et al. 2023).

We lack landscape-scale observations of meteorology and many other important environmental properties, so it is typically challenging or impossible to setup a single "best" model without a degree of trial-and-error. Therefore, model parameters are often estimated through calibration. Equifinality arises during calibration when different parameter sets yield similar realizations of observable phenomena (Beven 1993, 2006, Ebel and Loague 2006). Recognizing that equifinality may preclude the possibility of picking a single "best" parameter set, some modelers advocate for using a "behavioral" ensemble based on subjective goodness-of-fit criteria in a generalized likelihood uncertainty estimation (GLUE) framework (Spear and Hornberger 1980, Beven and Binley 1992, Her and Chaubey 2015, Vrugt and Beven 2018).

70

Equifinality implies process uncertainty (Grayson et al. 1992, Khatami et al. 2019). For example, total evapotranspiration (ET) is the sum of overstory and understory transpiration, interception loss, soil evaporation, snow sublimation, and other vapor fluxes; equifinal parameter sets may produce the same total ET with different partitioning between constituent fluxes (Franks et al. 1997, Birkel et al. 2024). Because each vapor flux component can respond differently to disturbance (Goeking and Tarboton 2020), we hypothesize that equifinal parameter sets may produce divergent predictions when the model is perturbed beyond the calibration space. (Seibert and McDonnell 2010, Melsen et al. 2018).

We illustrate the hypothesized interaction of equifinality, disturbance, and bias (non)stationarity using a conceptual water balance model (Fig. 1). Example models of the pre-disturbance water balance each achieve the same mean pre-disturbance streamflow (Q), which is forced to approximately match Q observations through model calibration. Due to equifinality, there is residual uncertainty in the bias-corrected total precipitation (P) and the partitioning of ET between transpiration and interception from tree canopies (ET_{Tree}) and other vapor fluxes (ET_{Other}, e.g., understory ET and soil evaporation). When a disturbance such as a fire reduces ET_{Tree}, the streamflow response is sensitive to the initial ET_{Tree} magnitude (and hence the potential ET reduction) as well as the degree to which ET_{Other} responds to increased soil water availability. The three examples show cases where ET_{Other} does not respond to the disturbance (Model 1), increased ET_{Other} fully compensates for reduced ET_{Tree} (Model 2), or increased ET_{Other} only partly compensates for reduced ET_{Tree} (Model 3). Intuitively, these hypothetical model responses are connected to the pre-disturbance balance of ET_{Tree} and ET_{Other}, which primes some models to predict a larger or smaller compensation effect. Over- or under-estimation of the resultant streamflow change (ΔQ) manifests as a positive or negative "bias shift" after disturbance. The bias shift metric, as defined here, is a special discrete case of the more general concept of nonstationarity. In a system with changes that occur over longer time periods (in contrast to the discrete disturbance shown in Fig. 1), a different stationarity metric would be necessary to account for incremental changes. In the present study, zero bias shift after disturbance implies stationary error overall.

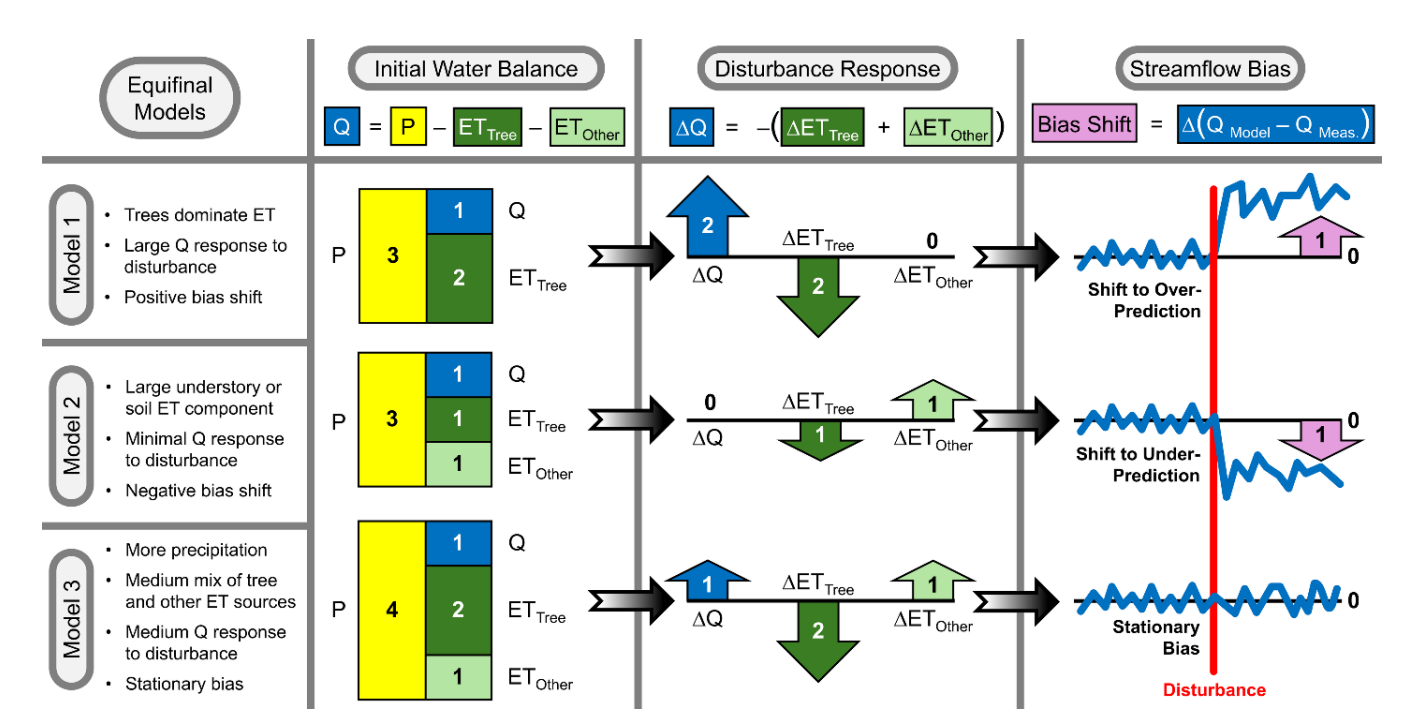


Figure 1: Conceptual model illustrating how equifinality in the modeled water balance may lead to uncertainty in the streamflow response to disturbance, and how we expect this to manifest in a measurable "bias shift" after a discrete disturbance. Numbers are indicative and not intended to represent actual disturbance magnitudes. In the "initial water balance" panel, we assume that all three models closely match pre-disturbance streamflow, with uncertain precipitation and evapotranspiration (ET) components counterbalanced to produce $Q_{Observed} = Q_{Modeled} = 1$ (normalized annual units). After a disturbance (e.g., a wildfire) reduces ET_{Tree} , the different models predict various degrees of streamflow change, which is mediated by the potential for compensating increases in ET_{Other} (e.g., soil evaporation and understory ET). In the "disturbance response" panel, the arrows illustrate the direction and magnitude of the water balance changes predicted by each model. In the "streamflow bias" panel, the resulting model predictions are compared to measured streamflow, showing how some models could exhibit a bias after disturbance due to uncertain estimation of water balance changes. In this hypothetical example, we assume that $Q_{Observed}$ increases by 1 unit after disturbance, matching the prediction of Model 3.

We build on this conceptual example of the interaction between equifinality, disturbance, and nonstationarity (Fig. 1) to consider how the bias shift metric can help select parameter sets with enhanced physical fidelity and greater predictive confidence. The initial water balance of Model 1 is dominated by ET_{Tree} , leading to a large streamflow gain and a positive bias shift (tendency toward over-prediction of post-disturbance streamflow). Conversely, Model 2 has a large ET_{Other} component, which compensates for the comparatively small reduction in ET_{Tree} , leading to a negligible streamflow gain and a negative bias shift (tendency toward under-prediction of post-disturbance streamflow). Finally, Model 3 has more precipitation than the other models and a more balanced combination of ET_{Tree} and ET_{Other} , leading to a medium streamflow gain and stationary bias. In this case, Model 3 should be preferred due to its negligible bias shift, which would help achieve a better prediction of ΔET and ΔQ and also help constrain uncertainty in the underlying parameterization.

As illustrated in Fig. 1, meteorological uncertainty (e.g., a precipitation bias) can interact with uncertain model parameterizations, contributing to uncertainty in the streamflow response to disturbance (Elsner et al. 2014). Basin-scale meteorology data are highly uncertain in mountain regions (e.g., Lundquist et al. 2015, Henn et al. 2018, Schreiner-McGraw and Ajami 2022), and whatever assumptions are made about the meteorology can cause compensating inaccuracies with other calibrated parameters (Elsner et al. 2014). For example, overestimating basin-scale precipitation may cause the model to simulate a larger ET_{Tree} component and a corresponding large change in post-fire water balance partitioning (Model 3 in Fig. 1), whereas underestimating basin-scale precipitation could limit the predicted post-fire streamflow change since the pre-fire P-Q residual is smaller (Models 1-2 in Fig. 1). From a Bayesian perspective, we can view the data and model as a combined inferential system, which enables us to constrain uncertainty in the interactions between uncertain meteorology and uncertain hydrology by generating suitable ensemble samples (Kavetski et al. 2003). Thus, uncertainty in the meteorological forcing data will contribute to uncertainty in our estimate of post-fire streamflow changes.

120

125

130

135

140

145

Equifinality has been neglected in many process-based simulations of environmental disturbance. In contemporary studies, single parameter sets are sometimes used with or without site-specific calibration (e.g., Furniss et al. 2023, Abolafia-Rosenzweig et al. 2024). When parameter ensembles are used, uncertainty propagation is commonly limited to subsurface parameters and meteorological biases (e.g., Shields and Tague 2012, Saksa et al. 2017, Boisramé et al. 2019). We expect that latent uncertainty in vegetation parameters may contribute an unconstrained source of uncertainty in studies of ecohydrological disturbance that do not account for vegetation parameter equifinality. Conversely, model equifinality can be reduced by leveraging additional types of information beyond traditional streamflow calibration metrics (Kelleher et al. 2017). One unexplored approach to equifinality reduction is evaluating the stationarity of model biases after environmental disturbance (e.g., bias shift in Figure 1), which we consider here.

In this study, we leverage a large wildfire as a "natural experiment" to test the hypothesis that quantifying stationarity across pre- and post-disturbance periods can reduce equifinality and improve the predictive confidence of a process-based hydrological model. Specifically, we apply the Distributed Hydrology Soil Vegetation Model (DHSVM, Wigmosta et al. 1994) to simulate streamflow changes attributable to the Creek Fire in the Sierra Nevada mountains (California, USA), which burned 56% of the forested area in our 4,244 km² study watershed (Stephens et al. 2022, Ayars et al. 2023). We expect that this drastic landscape-scale environmental disturbance should have a clear impact on regional-scale water fluxes, providing a natural experiment to test whether ecohydrological model process representations are robust to environmental disturbance. We leverage a multi-objective calibration of vegetation, snow, subsurface, and meteorological bias-correction parameters to address two research questions:

- (1) How does calibration equifinality impact process-based simulations of the hydrological response to a megafire?
- (2) Can we reduce equifinality and uncertainty by testing the model's representation of hydrological change?

150 **2 Methods**

155

160

2.1 Study Area and Data

Our study watershed encompasses the Upper San Joaquin River Basin above the outlet of Millerton Lake, a total of 4,244 km² with an elevation range of 100 to 4,200 m (Fig. 2A). The 2020 Creek Fire burnt 1,540 km² of mixed conifer and scrub forest, including 1,481 km² within the study watershed (56% of the forested watershed area). Landsat-based data from Monitoring Trends in Burn Severity (MTBS, Fig. 2B) indicate that 16% of the Creek Fire exhibited high burn severity and 30% exhibited moderate severity (Eidenshink et al. 2007, MTBS Project 2022). However, using a longer time period for pre- and post-fire imagery, Stephens et al. (2022) estimate 41% high severity and 35% moderate severity, illustrating the proliferation of uncertainty in disturbance assessments.

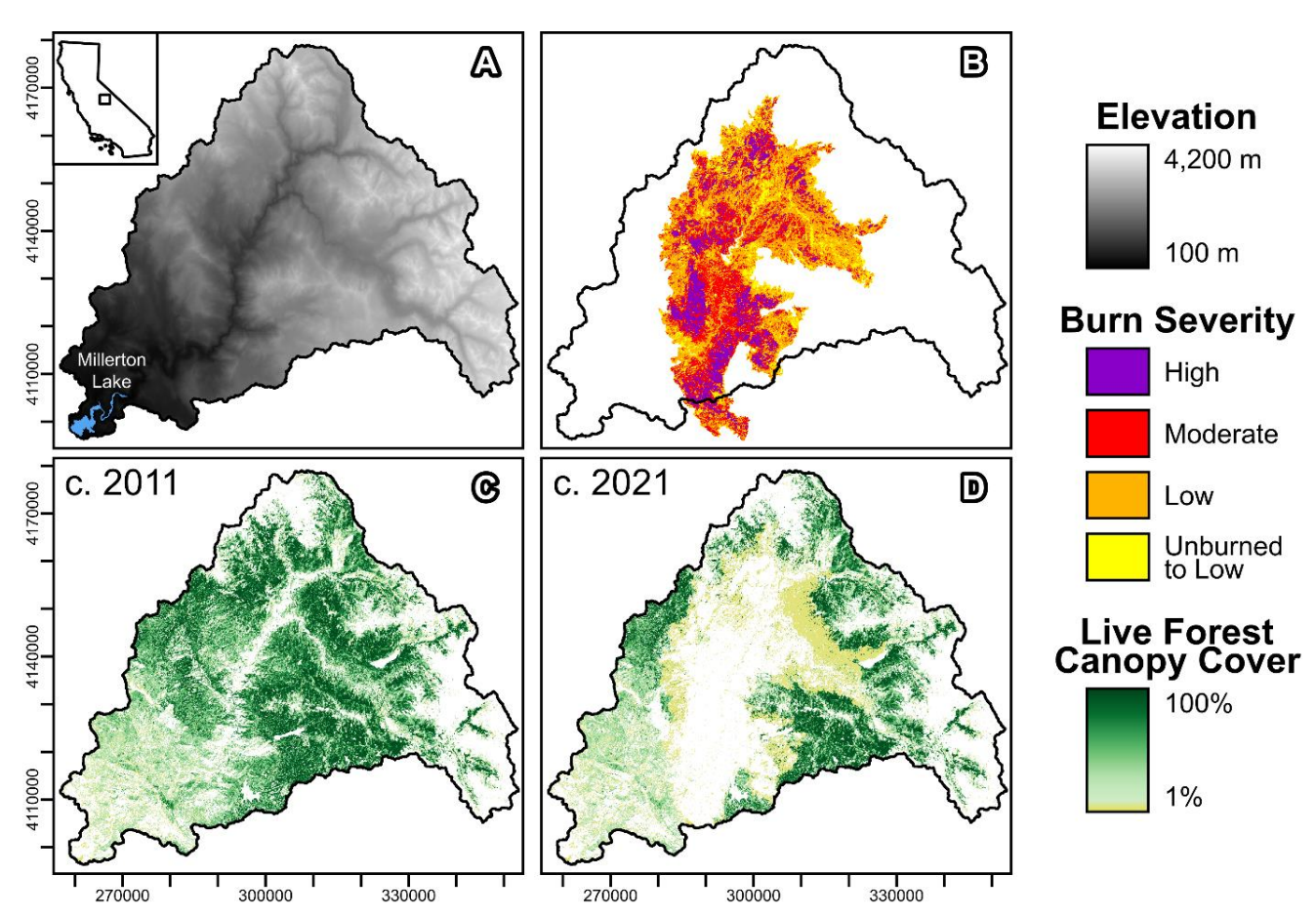


Figure 2: Maps of the study watershed: (A) elevation and watershed location in the U.S. State of California, (B) 2020 Creek Fire burn severity, (C) pre-fire and (D) post-fire forest canopy cover. Tick marks indicate 10 km intervals.

We represent fire disturbance in DHSVM by adjusting maps of vegetation properties. Canopy cover maps are projected to our selected DHSVM resolution of 90 m using nearest-neighbor resampling to preserve the categorical attribute of tree presence/absence. The Landsat-based RCMAP data provide yearly fractional cover estimates for trees and shrub/herbaceous vegetation at 30 m resolution (Rigge et al. 2021a,b). We use the 2011-era RCMAP data as a pre-fire baseline and the 2021-era RCMAP data to capture the effects of the 2020 Creek Fire (Fig. 2C-D). We also update the vegetation maps in 2013, 2014, and 2018 to reflect smaller fires in those years. The DHSVM vegetation maps are updated on October 1st in the year of a fire, i.e., about one month after the September 2020 Creek Fire ignition. The October 1st date is used for annual model updates because this date represents the start of a new water year, and Sierra Nevada watersheds are typically near their driest condition around this time of year, which limits the impact of model changes on simulated hydrological fluxes. Additionally, fires typically burn in the late summer in the Sierra Nevada, so the October 1st date is close to the typical end of the fire season. However, studies focused on short-term post-fire effects may need to update vegetation maps on the dates immediately after each fire, or even multiple times as a fire progresses (e.g., the Creek Fire burned for several months). Vegetation is classified based on the species (when available) or functional type (e.g., mixed conifer forest) using Landfire data (2022), and abiotic land surface classes are derived from NLCD (Dewitz and U.S. Geological Survey 2019). Landfire and RCMAP provide tree and shrub height data, respectively. Tree leaf area index (LAI) is estimated empirically from fractional cover following Pomeroy et al. (2002), which is reproduced as Eq. (1) of Goeking and Tarboton (2022b). Satellite-based optical LAI estimates are highly uncertain in mountain environments due to saturation at the high LAI values often present in mature conifer forests and the inability to resolve 3-dimensional canopy structure that controls LAI (Zolkos et al. 2013, Winsemius et al. 2024). Thus, we use the fractional cover relationship to constrain the spatial patterning of LAI, but the uncertain LAI magnitude is estimated heuristically through calibration. Vegetation transpiration is calculated by DHSVM based on the vegetation type and local weather, soil moisture, and light in each grid cell (Wigmosta et al. 1994). Baseline values of minimum stomatal resistance are estimated from species-level field studies as detailed in the Supporting Information of Boardman et al. (2025) and refined by calibration relative to baseline (Sect. 2.2).

165

170

180

185

190

195

Spatial maps and parameter values for DHSVM are collated from a wide range of literature and field studies, as detailed in Boardman et al. (2025). We briefly summarize key setup procedures here. Subsurface properties are estimated by disaggregating regional soil survey databases (Gupta et al. 2022, Soil Survey Staff 2022) using Random Forest models trained on topographic metrics (Breiman et al. 2002). In the updated version of DHSVM used here, streamflow in channels is bidirectionally coupled to the groundwater level in each grid cell, and the maximum network extent is derived from the National Hydrography Dataset (U.S. Geological Survey 2019) with channel geometry from regional regressions (Bieger et al. 2015). Meteorological data from gridMET (Abatzoglou 2013) are disaggregated to a 3-hour timestep using MetSim (Bennett et al. 2020). Modeled snowfall is distributed in proportion to the pixel-wise maximum observed snow water equivalent (SWE) pattern derived from Airborne Snow Observatory (ASO) data in the study watershed (Painter et al. 2016), which implicitly accounts for snow transport (Vögeli et al. 2016). Regional snow/rain partitioning parameters are adopted from Sun et al. (2019).

2.2 Model Calibration

200 We calibrate 14 sensitive and uncertain parameters in DHSVM that control aspects of the meteorology, vegetation, subsurface, and snowpack dynamics (Table 1, Supplemental Figure S4). While most of these parameters are widely recognized as suitable for calibration (Cuo et al. 2011, Du et al. 2014), precipitation and temperature biases are less frequently included in the calibration of distributed process-based models despite considerable uncertainty in gridded meteorological data. Among gridded meteorological datasets, there is a mean relative difference of 21% for annual precipitation in our study watershed 205 (Henn et al. 2018), and misestimation of large storms can lead to yearly biases of about 20% across the Sierra Nevada (Lundquist et al. 2015). Similarly, gridded meteorological datasets have mean air temperature differences as large as ±8 °C in the Sierra Nevada, and basin-average uncertainty is lower but still on the order of several °C (Schreiner-McGraw and Ajami 2022). Compensation between unknown errors in the meteorological data, model structure, and parameter calibration can potentially contribute to spurious goodness-of-fit metrics with hidden physical deficiencies. This is especially the case in 210 environmental disturbance studies, as we expect that interactions between meteorological uncertainty and parameter equifinality may contribute to the overall uncertainty of disturbance simulations (Fig. 1). Critically, this uncertainty would remain hidden if meteorological biases were assumed to be negligible. Because perfectly resolving the weather data with infinite precision is not feasible across a large, rugged mountain region, the robust approach is to propagate meteorological uncertainty into our final results (the post-fire hydrological change in this case), so that our conclusions include the quantified 215 uncertainty caused by the model-data-calibration interaction. We view the combined meteorological data and hydrological model as a single inferential system, thereby acknowledging that the meteorological data themselves are based on various uncertain observations and empirical model assumptions (Abatzoglou 2013). In a Bayesian context, the goal of our calibration can be understood as sampling the probability of the calibration data (streamflow and snowpack observations) given a particular combination of model parameters and meteorological assumptions: P(streamflow + snowpack observations | model 220 + meteorology). Because we lack a closed-form likelihood function for spatially distributed hydrological models like DHSVM, we estimate the unknown parameters of this whole weather-model system using an informal approximation based on traditional hydrological model calibration objective functions (Beven and Binley 1992).

Category	Parameter	Range	Primary Process Controls
Meteorology	Precipitation Bias	±25%	Net water balance input, interannual variability in water balance, snowpack accumulation
	Temperature Bias	±4 °C	Snow/rain partitioning, snowpack accumulation and melt, potential evapotranspiration (PET)
	Temperature Lapse Rate Bias	-8 to -2 °C/km	Spatial distribution of snowpack and PET
Vegetation	Tree Fractional Cover	50% to 200% of baseline, each cell ≤ 100% cover	Canopy interception and transpiration, understory and snowpack shading
	Tree Leaf Area Index (LAI)	50% to 200% of baseline	Canopy interception capacity, overstory transpiration
	Minimum Stomatal Resistance	50% to 200% of baseline	Overstory and understory transpiration
Subsurface	Soil Depth	1 to 10 m	Lateral transmissivity, root zone groundwater access, storage capacity
	Hydraulic Conductivity	10^{-5} to 10^{-2} m/s	Lateral transmissivity, vertical recharge rate (by anisotropy ratio), surface/subsurface flow partitioning
	Exponential Decrease in Conductivity	10 ⁻³ to 10 ⁰ [unitless]	Lateral transmissivity, vertical conductivity profile, baseflow recession, water table depth
	Porosity	0.3 to 0.6 [fractional]	Dynamic storage range, water table response to infiltration
	Field Capacity	0.1 to 0.4 [fractional]	Dynamic storage range, soil water retention, plant available water
Snow	Albedo Decay Rate (Accumulation)	0.7 to 0.99 [unitless]	Snowpack energy balance, maximum accumulation
	Albedo Decay Rate (Melt Season)	-0.3 to 0.0 relative to accumulation	Snowpack energy balance, snowmelt rate, snow cover duration
	Albedo Reset Snowfall Scale	10^{-4} to 10^0 m SWE	Relative albedo increase associated with new snowfall of varying depth

Table 1: Prior ranges and process controls of DHSVM parameters calibrated in this study. All vegetation and subsurface parameters listed here are defined by spatially variable maps, and calibration ranges determine the area-average value around which the pattern is rescaled.

Multiple parameters combine to control simulated processes. For example, area-average LAI (related to total interception loss) is the product of tree-scale LAI with grid-scale fractional cover. Tree transpiration is determined by fractional cover, LAI, stomatal resistance, available soil water (related to subsurface parameters), and other factors. Lateral transmissivity in the saturated subsurface is controlled by three parameters: soil depth, surface hydraulic conductivity, and the exponential decrease in conductivity with depth. Cross-compensation among interrelated parameters thus contributes to equifinality. Within our 14-dimensional calibration space, 23 parameter pairs have correlations that are significant at p < 0.05 (Supplemental Fig. S1). Furthermore, perturbing one aspect of the model can lead to cascading effects due to the coupling of ecohydrological processes and spatial water connectivity in the model. For example, lateral hydraulic conductivity is coupled to vertical conductivity by anisotropy ratios dependent on the soil textural classification (Fan and Miguez-Macho 2011), so calibrating lateral conductivity

230

also influences groundwater recharge rates from losing stream reaches, which in turn can affect soil evaporation and transpiration from riparian trees. Spatial heterogeneity in modeled soil and vegetation properties (Sect. 2.1) further complicates all of these interactions, e.g., different parts of the landscape are relatively more sensitive to calibration of different parameters depending on the baseline map patterns.

240

245

250

255

260

Given the complexity of expected interactions, we define seven objective functions to constrain parameters based on different hydrological signatures (Table 2). Streamflow is estimated at the outlet of Millerton Lake (Fig. 2) by reconstructing observations to remove the effects of artificial flow regulation (California DWR 2024). Millerton Lake unimpaired outflows are estimated assuming sub-daily surface routing times by summing the daily change in storage, canal and dam releases, surface evaporation, and storage changes at eight smaller upstream reservoirs (Huang and Kadir 2016). Note that the reconstructed streamflow timeseries used in this study (called "full natural flow" by the California Data Exchange Center) is based on an explicit mass balance equation applied directly to the respective storage and flow measurements, not model output, unlike various other meanings of "natural flow" that are sometimes applied to California water datasets (Huang and Kadir 2016). The reconstructed streamflow timeseries (hereafter "observed streamflow") represents the actual effects of the Creek Fire (and other disturbances) because the reconstruction procedure is directly based on measurements at specific diversion, storage, and outflow points, which are directly responsive to the basin hydrological conditions. Three objective functions are based on a cleaned version of this daily streamflow timeseries (spurious negative values during low-flow periods and other missing values are imputed). Two objective functions similarly target annual percent error in the annual water yield and the April-July water yield, which is a well-established benchmark for snowmelt runoff modeling in the Sierra Nevada (Pagano et al. 2004). Two objective functions are based on the eight-year (2017-2024), 30-survey database of ASO SWE maps in the study area, targeting both the spatial distribution at the 90 m grid scale and the percent error in total volume across surveys. Hydrograph and water yield objectives are calculated for water years 2015-2024, which includes six years before and four years after the Creek Fire. By calibrating across this disturbance (vegetation maps updated during calibration), we automatically reject parameter sets that fail to provide reasonably accurate estimates of both pre- and post-fire streamflow.

Category	Objective Function	Best Value	Worst Value	Target Hydrological Signatures
Daily Streamflow (2015-2024)	NSE	0.89	0.80	Hydrograph shape (high flows), rainfall-runoff response, snow/rain partitioning, peak flow and recession timing
	Log-Scaled NSE	0.85	0.80	Hydrograph shape (low flows), baseflow recession characteristics, multi-year storage/deficit effects
	>95 th -Percentile RMSE	26 m ³ /s	74 m ³ /s	High flow magnitude, shape of flow duration curve independent of timing
Water Yield (2015-2024)	Yearly MAPE	4%	9%	Bulk water balance, interannual variability across wet and dry years
	April-July MAPE	7%	10%	Interannual variability in snowmelt runoff efficiency and timing
Snow Maps (30 ASO	Pixel-Wise SWE RMSE	0.23 m	0.25 m	Spatial distribution of snow accumulation and ablation, absolute magnitude of SWE in different years
Surveys, 2017-2024)	Total SWE Volume MAPE	18%	32%	Evolution of snowpack volume between surveys, interannual variability

Table 2: Calibration objective functions used in this study with descriptions of the primary hydrological signatures constrained by each objective. The best (worst) value given here is the lowest (highest) error achieved by any of the Pareto-efficient parameter sets in our calibrated 30-member behavioral ensemble. NSE = Nash Sutcliffe Efficiency, RMSE = root mean square error, MAPE = mean absolute percent error.

To efficiently sample behavioral parameter sets from the 14-dimensonal space of potential interactions, we apply a multiobjective Bayesian optimization scheme (Jones et al. 1998). After an initial Latin hypercube sample of 320 parameter sets
(Dupuy et al. 2015), we perform parallel particle swarm optimization (Kennedy and Eberhart 1995, Zambrano-Bigiarini et al.
2013) using the expected hypervolume indicator (Emmerich et al. 2011, Binois and Picheny 2019) to sample promising
parameter sets based on Gaussian Process surrogate models of the objective function response surfaces (Roustant et al. 2012).
After six optimization generations, we have tested a total of 600 parameter sets (n.b. this requires ~950 days of CPU time on
2.5 GHz servers, but the elapsed wall-clock time is several weeks because multiple parameter sets are tested in parallel). While
this number of tested parameter sets may seem small by conventional standards considering the 14-dimensional search space,
we note that each new parameter sample is selected after an independent optimization procedure using 100 to 1,000 particle
swarm samples from the objective function surrogate models. Thus, our overall calibration explores the objective function
tradeoffs across more than 160,000 parameter sets, but only 600 of these are actually tested in DHSVM. Because testing
hundreds of thousands of parameter sets directly in DHSVM would require prohibitive amounts of computational expense,
this Bayesian surrogate optimization procedure is essential for efficiently selecting parameter sets that have the best likelihood
of substantially improving the Pareto frontier.

As expected for any high-dimensional multi-objective optimization problem, there is no single "best" parameter set. Rather, the behavioral parameter sets constitute a Pareto frontier, with some performing slightly better at one objective and worse at another. One way of understanding this phenomenon is that the parameter sets with the absolute highest values for any single objective are overfitting to noise in the data, while parameters that perform reasonably well at a variety of objectives are

intuitively more likely to capture salient hydrological information. Narrowing the range of acceptable parameter sets requires case-by-case determination of what skill level is satisfactory for a particular watershed-model combination because a higher skill might be achieved in hydroclimates that are conceptually simpler to simulate. At the same time, it is necessary to retain enough parameter diversity to explore our research questions related to the interaction between equifinality and disturbance. Based on prior experience modeling with DHSVM in the Sierra Nevada (e.g., Boardman et al. 2025), we find that the best model skill we can generally achieve is around a daily NSE of approximately 0.8 or higher and yearly error of approximately 10% or lower. Any single criteria is insufficient for narrowing the parameter space to a reasonable fraction of the total calibration space. For example, over 30% of all tested parameter sets have daily NSE > 0.8 (none have NSE > 0.9), but some of these high-NSE parameter sets are clearly inferior, e.g., with yearly MAPE as high as 35%. Combining multiple thresholds, we find that 48 parameter sets qualify as "behavioral" by satisfying daily NSE > 0.8, daily log NSE > 0.8, yearly MAPE < 10%, April-July MAPE < 10%, and Pareto-efficiency across all objectives. We do not directly apply thresholds to the snow calibration metrics because the variability of these objective functions is already strongly constrained within the behavioral ensemble (e.g., the SWE RMSE coefficient of variation is 2% within the behavioral ensemble compared to 59% across all 600 parameter sets). Nevertheless, snow-based objective functions still constrain the behavioral ensemble because all behavioral parameter sets must be Pareto-efficient across all seven objectives. Some behavioral models have very similar parameter sets, so for efficiency we further select 30 diverse samples by iteratively choosing the behavioral parameter set with the maximum mean parameter separation from previously selected samples. These 30 parameter sets define the behavioral DHSVM ensemble referenced hereafter. We note that our conclusions are robust to random sub-selection of fewer models, as long as at least ~10 parameter sets are used (Supplemental Fig. S2). We validate the performance of the selected parameter sets by simulating the 10 year period prior to the calibration period, i.e., water years 2005-2014, using the same objective functions.

290

295

300

305

310

315

To test whether our results are sensitive to our choice of a calibration period spanning a major disturbance, we repeat the entire calibration procedure over the time period immediately before the Creek Fire (water years 2011-2020). Unlike our primary calibration, which spans 6 years before the fire and 4 years after the fire, all 10 years of the "pre-fire calibration" have negligible change in the model vegetation maps. The pre-fire calibration is initialized with the same Latin hypercube sample of 320 random parameter sets, after which we perform six generations of multi-objective Bayesian optimization following the same procedures as the primary calibration discussed previously, and we select behavioral parameter sets using the same objective function criteria. Parameter sets resulting from this pre-fire calibration are completely independent from our primary calibration, so we use these results to test whether the model yields similar results when calibrated on a period without major vegetation map updates.

2.3 Disturbance Simulations

320

325

330

335

We investigate the ecohydrological effects of the Creek Fire by comparing model simulations using dynamic and static vegetation maps to quantify the fire effect relative to a no-fire control scenario. For each of the 30 DHSVM parameter sets, we simulate streamflow for the past 20 years (water years 2005-2024) with either static 2011-era vegetation maps or dynamic vegetation maps updated in 2013, 2014, 2018, and 2020. The 2020 Creek Fire accounts for most of the vegetation disturbance in the study area, with a 42% reduction in watershed-average RCMAP tree fractional cover compared to 2-3% reductions associated with the 2013, 2014, and 2018 fires. Differences between fire-aware (dynamic vegetation) and no-fire control (static vegetation) simulations define the modeled disturbance effect. In addition to comparing daily streamflow, we also compare annual water yield and ET fluxes between fire-aware and no-fire control scenarios.

2.4 Detecting and Correcting Nonstationarity

We calculate a "bias shift" metric by comparing observed streamflow with modeled streamflow from the fire-aware (dynamic vegetation) simulations. The bias shift metric is useful in two contexts. First, it is useful for understanding and refining the behavior of models, potentially including reducing equifinality by selecting models with near-stationary bias. Second, it is useful for refining our prediction of the real-world hydrological response to a disturbance by estimating what a hypothetical model with stationary error would have predicted.

The 30-member behavioral DHSVM ensemble has a reasonably small mean streamflow bias for the overall 2005-2024 evaluation period (interquartile range among parameter sets of $\pm 2\%$). However, some parameter sets have different mean streamflow biases on pre- and post-fire periods, congruent with our conceptual model in Fig. 1. We theorize that over- or under-estimation of the disturbance effect on streamflow may result in a matching positive or negative bias shift after disturbance, defined as the difference in mean streamflow bias between post-fire and pre-fire periods:

$$Bias Shift = (\overline{Q_{Model}} - \overline{Q_{Meas}})_{Post-Fire} - (\overline{Q_{Model}} - \overline{Q_{Meas}})_{Pre-Fire}$$
 (1)

340 We correct for the bias shift of different parameter sets by developing a "metamodel," i.e., a statistical model trained on DHSVM outputs. The bias shift metric, Eq. (1), is averaged across multiple years, whereas we expect that each individual year may have a larger or smaller streamflow response due to variable interactions between climate and vegetation. In the case that the streamflow response is purely energy-limited (P >> ET), we would expect the same post-fire streamflow gain in all years; conversely, in a water-limited case (P closer to ET magnitude) we would expect a 1:1 scaling between annual precipitation and the post-fire streamflow gain. Between these two endmember scenarios, we expect that the magnitude of the simulated streamflow change in any particular year may be offset and/or fractionally re-scaled relative to the mean multi-year streamflow change. Thus, we posit a linear relationship between the multi-year mean bias shift and the simulated streamflow response to fire in any particular year, ΔQ_{Fire}. The linear relationship between bias shift and yearly ΔQ_{Fire} is supported by graphical analysis

of bivariate scatterplots, as illustrated subsequently in Fig. 5. In other watersheds or disturbance scenarios, it might be necessary to posit a nonlinear relationship with the bias shift, which could again be detected from analogous bivariate scatterplots.

In a Bayesian statistical framework, we treat each DHSVM parameter set as an independent realization of the possible postfire response, with a stochastic error term describing scatter in the hypothesized linear relationship between bias shift and ΔQ_{Fire} . We define the metamodel using a normal distribution with mean determined by the linear bias shift vs. ΔQ_{Fire} relationship and uncertainty defined by the sample standard deviation σ , which can be expressed in Bayesian sampling notation as:

$$\Delta Q_{Fire} \sim normal(c_0 + c_1 * Bias Shift, \sigma)$$
 (2)

To estimate the values of c_0 , c_1 , and σ (with quantified uncertainty in all three parameters), we generate 1,000 Bayesian samples using the Hamiltonian Monte Carlo algorithm with two chains (500 samples per chain) after 10,000 warmup iterations (Stan Development Team 2023). The metamodel is fit using all 30 pairs of bias shift and ΔQ_{Fire} values calculated for each parameter set in the behavioral DHSVM ensemble, with c_0 , c_1 , and σ re-fit for each of the four post-fire years. We subsequently generate a conditional prediction of ΔQ_{Fire} in each year by setting the bias shift equal to zero in Eq. (2), which yields a normal distribution with mean c_0 and standard deviation σ . Unlike simple least-squares linear regression, uncertainty in the metamodel parameters (c_0 , c_1 , and σ) is propagated into our conditional predictions through the Bayesian sampling routine, which considers 1,000 different combinations of plausible c_0 , c_1 , and σ values. Sampling the posterior distribution of Eq. (2) with bias shift set to zero yields a conditional distribution describing the expected post-fire streamflow change and uncertainty of a hypothetical DHSVM simulation with zero bias shift.

2.5 Empirical Regression Model

350

355

360

365

To compare statistical and process-based approaches to ecohydrological disturbance attribution, we also apply an empirical annual water balance model using Bayesian multiple linear regression. We posit a simple four-parameter lumped empirical model that estimates the annual runoff efficiency (Q / P) as a linear function of annual precipitation (P), the prior year's streamflow (Q_{LastYear}) to account for multi-year storage or deficit effects, and the aridity index calculated from annual potential evapotranspiration (PET / P). Note that the annual PET used in the empirical water balance model is pre-calculated as part of the gridMET dataset (Abatzoglou 2013) from Penman-Monteith reference evapotranspiration, but PET is calculated separately within the DHSVM evapotranspiration module (Wigmosta et al. 1994), similarly using a Penman-Monteith implementation. The structure of the empirical model is adapted from a similar regression approach applied to analyze seasonal water supply in adjacent watersheds (Boardman et al. 2024). We assume that each year's actual runoff efficiency is randomly sampled from a normal distribution with standard deviation σ and mean defined by the linear model, expressed analogously to Eq. (2) in Bayesian sampling notation:

$$\frac{Q}{P} \sim normal\left(c_0 + c_1 * P + c_2 * Q_{LastYear} + c_3 * \frac{PET}{P}, \sigma\right) \tag{3}$$

We constrain the empirical model using pre-fire data and compare its post-fire predictions with measured post-fire streamflow. Meteorological data required for Eq. (3) are aggregated from the same gridMET data used for DHSVM (Abatzoglou 2013) over water years 1980-2020. As for Eq. (2), we generate 1,000 Bayesian samples of the empirical model parameters (c_0 , c_1 , c_2 , and σ) using Hamiltonian Monte Carlo (Stan Development Team 2023). The empirical model achieves $R^2 = 0.91$ for annual variations in runoff efficiency across the 41-year fitting period. By sampling the model's posterior predictive distribution using meteorological data from 2021-2024, we generate 1,000 counterfactual estimates of annual streamflow in each of the post-fire years. The difference between measured post-fire streamflow and predicted streamflow from the stationary statistical model provides an estimate of the streamflow change attributable to disturbance.

3 Results

385

390

395

400

405

410

The behavioral ensemble of 30 calibrated DHSVM parameter sets all reproduce observed streamflow hydrographs with a close match to peak flow and low flow magnitudes, interannual variability, and seasonal timing (Table 2, Fig. 3). Daily NSE values for the 2015-2024 calibration period vary between 0.80 and 0.89 among the different parameter sets (log NSE 0.80 to 0.85), with similar statistics on the 2005-2014 validation period (NSE 0.76-0.88, log NSE 0.80-0.87). All behavioral parameter sets also achieve NSE of 0.80 to 0.89 and log-scale NSE of 0.76 to 0.84 considering just the four years after the Creek Fire, which is considered satisfactory because the model skill is similar on pre- and post-fire periods. Additionally, the post-fire daily NSE of at least 0.80 achieved by all behavioral DHSVM parameter sets is substantially higher than the post-fire daily NSE of -0.13 to 0.60 achieved by a different distributed hydrological model (with dynamic vegetation and other fire-aware updates) after a megafire in other Sierra Nevada sub-watersheds (Abolafia-Rosenzweig et al. 2024). Without the vegetation map updates, the behavioral ensemble performs significantly worse on the post-fire period, but streamflow skill is still reasonably high: the mean NSE is lower by 0.06 in the no-fire control scenario (p < 0.001, Welch one-sample t-test) and the mean log NSE is lower by 0.02 (p < 0.001). Furthermore, the no-fire control scenario yields a mean post-fire bias between -17% and -9% (static vegetation systematically underestimates post-fire streamflow), while in dynamic vegetation mode the mean post-fire bias varies between -9% and +6% (Supplemental Figure S3). Comparing fire-aware and no-fire counterfactual scenarios, the behavioral ensemble indicates a bulk streamflow increase of +2 to +17% after the Creek Fire (median +12%). DHSVM also indicates a shift towards earlier snowmelt runoff after the Creek Fire. Because our post-fire implementation only changes the vegetation maps (no change to modeled soil or snow albedo), the prediction of earlier snowmelt runoff is primarily a result of increased energy reaching the snowpack due to reduced canopy shading. This snowmelt timing effect is most noticeable in the 2023 water year, which was a year with extremely high snow accumulation (Marshall et al. 2024).

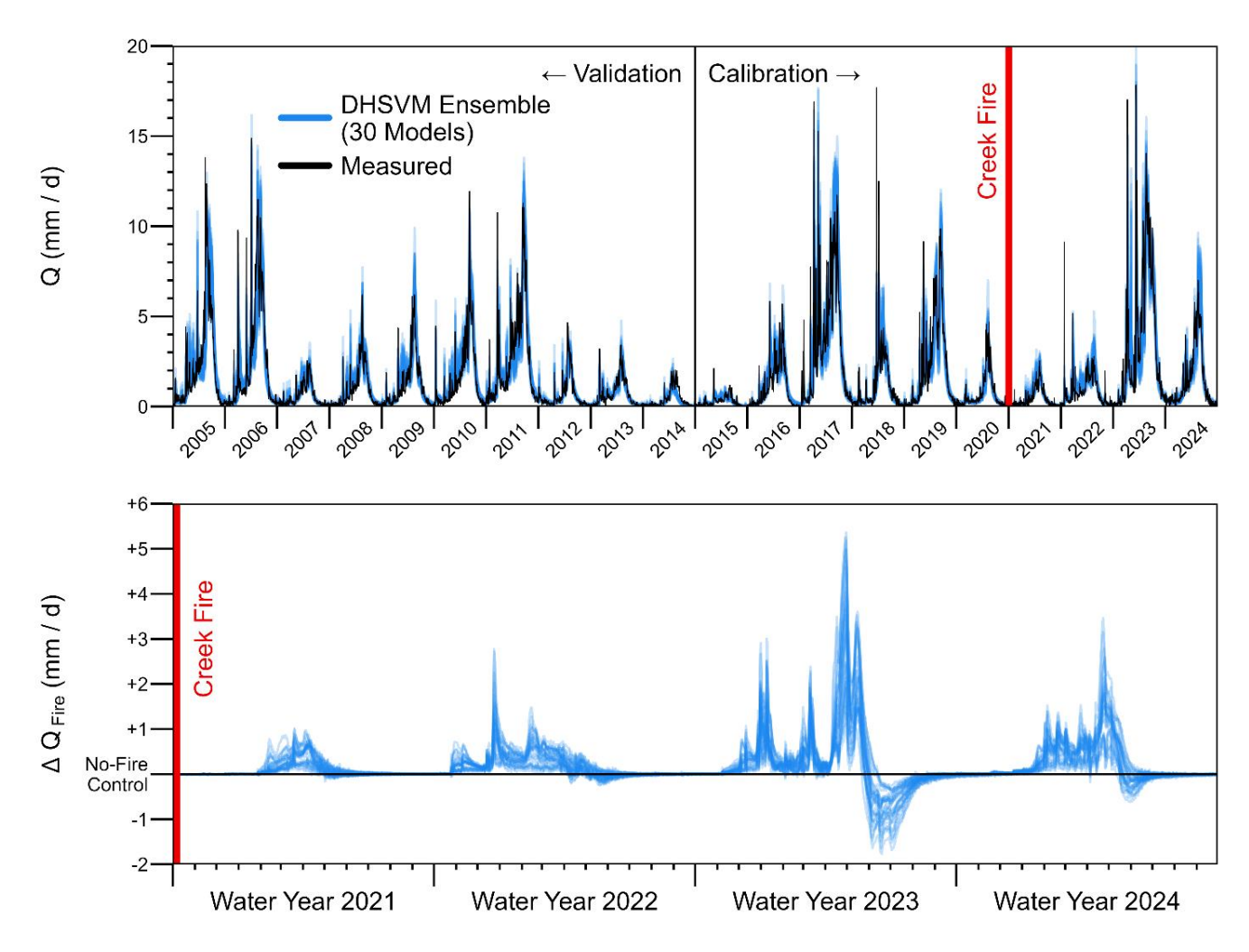


Figure 3: Modeled and measured daily streamflow hydrographs (top panel) and streamflow differences between fire-aware and nofire control simulations (bottom panel). Both panels show results from 30 calibrated "behavioral" parameter sets (Sect. 2.2).

Uncertainty in the streamflow response to disturbance is large relative to the size of the effect, even after a megafire. The difference in total post-fire streamflow volume between fire-aware and no-fire control scenarios has a coefficient of variation of 41%. Some parameter sets predict up to a 650% larger annual streamflow response than other parameter sets (inter-model range of +13 to +97 mm/yr). Relative uncertainty is higher in dry years, with the simulated streamflow response in 2021 varying between +3 mm/yr and +47 mm/yr across different parameter sets (1,400% range). The predicted streamflow change after the Creek Fire is on the same order of magnitude as stochastic error in the annual water balance (Supplemental Fig. S3), which intuitively explains why the disturbance response remains uncertain despite direct calibration of pre- and post-fire streamflow (Fig. 3).

Uncertainty in the post-fire streamflow response is linked to equifinality in modeled water balance fluxes (Figs. 1, 4). To qualify as "behavioral," parameter sets must satisfactorily estimate the annual water balance (MAPE < 10%), but the model can achieve this in different ways. Some parameter combinations suggest that transpiration and interception loss from vegetation accounts for up to 95% of total pre-fire ET, while others suggest a vegetation contribution as low as 77%, with the balance contributed by evaporation from abiotic surfaces (stream channels and soil, including rock above treeline). Relatively dense initial forests (high area-average LAI) are associated with large decreases in post-fire transpiration and interception loss (Pearson r = -0.92, p < 0.01). Low transmissivity is associated with increases in post-fire soil evaporation and channel evaporation (r = -0.99, p < 0.01, both variables log-transformed).

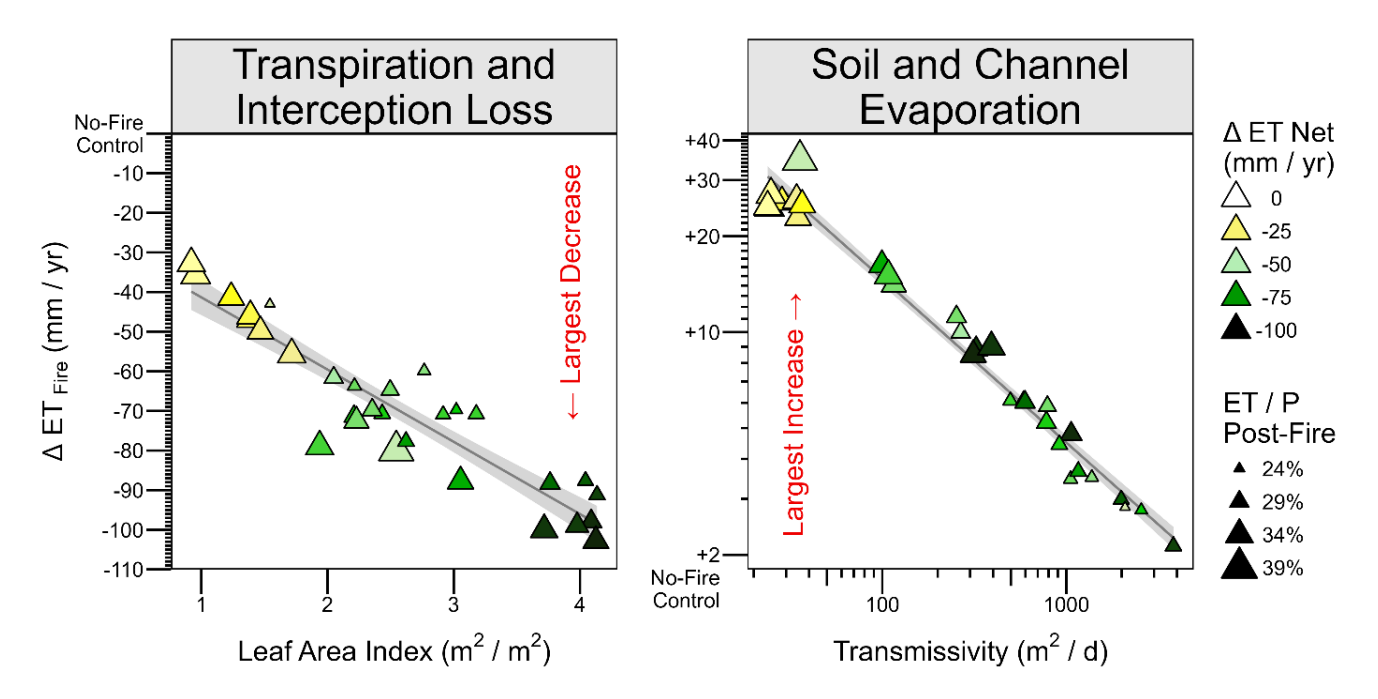


Figure 4: Difference in ET fluxes between fire-aware and no-fire control simulations visualized relative to model parameter uncertainty. Each point represents a single behavioral parameter set (N = 30) with all values spatially averaged within the watershed. The area-average leaf area index (LAI) is aggregated within the pre-fire forested area from maps of tree-scale LAI and grid-scale fractional cover, (both of which are calibrated, see Table 1), and the area-average transmissivity is aggregated from maps of soil depth, conductivity, and exponential decrease using the DHSVM transmissivity equations (all three of which are also calibrated, see Table 1). Trend lines indicate the least-squares fit and 90% confidence interval of the best-fit linear estimator.

Compensating errors in equifinal parameter sets can produce compounding discrepancies after disturbance. Not only do some parameter sets indicate much larger changes in individual fluxes, those with the smallest reductions in vegetation ET also exhibit the largest fractional compensation (up to 76%) from increased abiotic evaporation (r = 0.71, 0.01). A similar compensation between modeled overstory and understory ET components is illustrated by Boardman et al. (2025). Low calibrated transmissivity implies slower groundwater recharge and shallower flowpaths, contributing to higher soil

evaporation, which compensates for low vegetation ET. These parameter sets are primed for large increases in evaporation when soil moisture increases in de-forested areas after fire. Consequentially, there is a negative correlation (r = -0.93, p < 0.01) between the fraction of pre-fire ET contributed by abiotic evaporation and the magnitude of the post-fire net ET reduction.

Evaluating the model bias shift (Eq. 1) can help escape this morass of uncertainty. Across the 30-member behavioral ensemble, there is a strong correlation (r = 0.96-0.99 depending on year, p < 0.01) between the mean streamflow bias shift after disturbance and the annual streamflow change attributable to fire (Fig. 5). Lines in Fig. 5 correspond to Eq. (2), and the horizontal axis is defined by Eq. (1). Bayesian sampling of a linear model conditioned on zero bias shift yields an estimate of the uncertainty in the vertical intercept (Sect. 2.4), which is the predicted streamflow change of models with stationary bias.

Comparing the annual streamflow errors of models with positive or negative bias shift (Supplemental Fig. S3), we note that the positive-shift models tend to have more-positive errors on the pre-fire period compared to negative-shift models, but this stratification reverses after the Creek Fire. This reversal of model over- and under-prediction after disturbance is consistent with our conceptual model in Fig. 1. Additionally, as shown by the shape-size in Fig. 5, the models with the largest over-prediction have anomalously high overstory LAI, and vice versa, which is similarly consistent with the conceptualization of ET_{Tree} and ET_{Other} equifinality in Fig. 1.

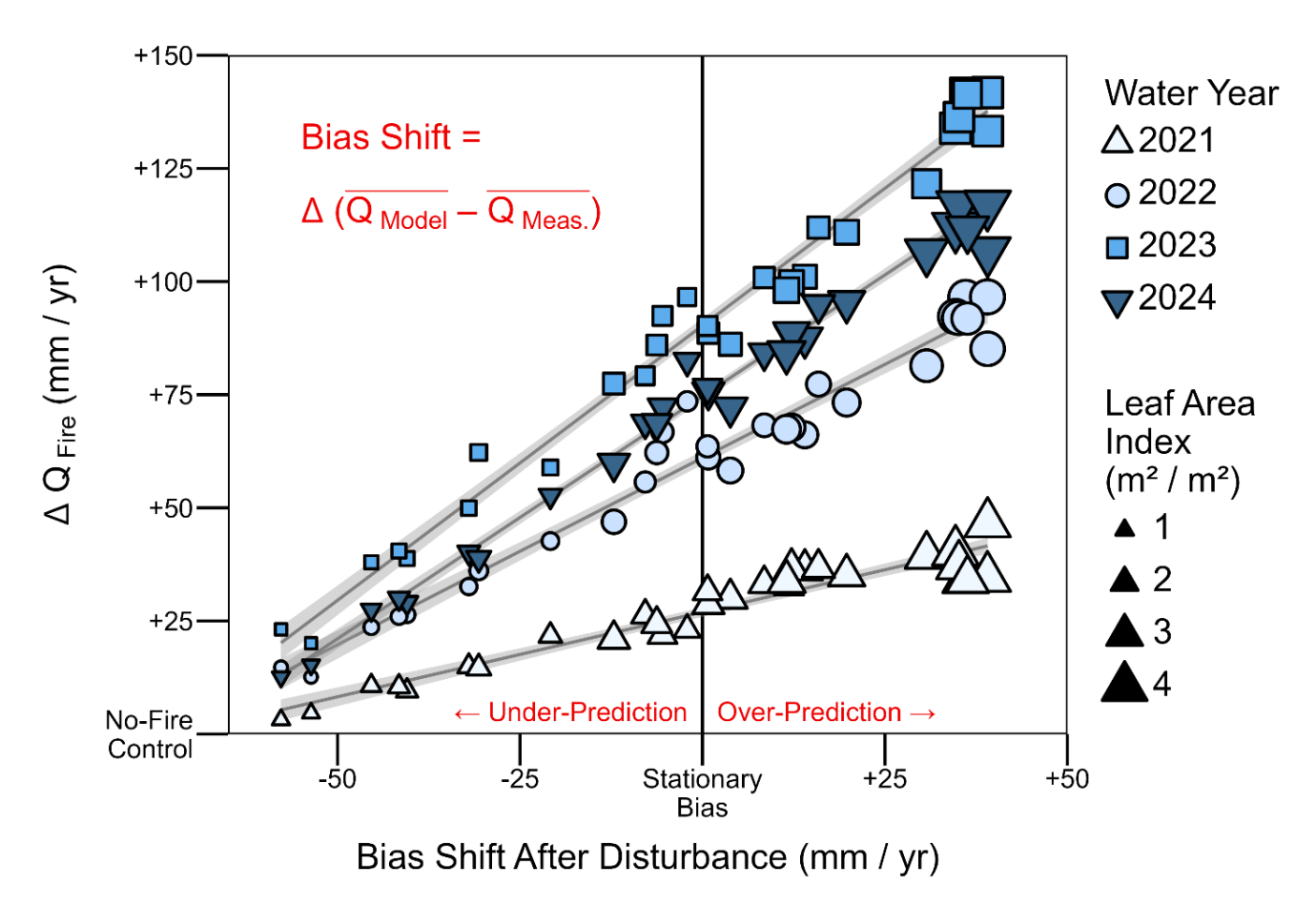


Figure 5: Annual post-fire streamflow change visualized relative to the mean bias shift after disturbance for all 30 parameter sets. Parameter sets with a shift towards overestimation predict a relatively large streamflow response to disturbance, and vice versa. Parameter sets with near-stationary bias are assumed to give the most accurate estimate of changes due to disturbance. Trend lines indicate the least-squares fit and 90% confidence interval of the best-fit linear estimator, distinct from the analogous Bayesian regression in Eq. (2), which also propagates parameter uncertainty.

Eight parameter sets result in near-stationary bias (shift less than ± 10 mm/yr). This eight-member "stationary sub-ensemble" demonstrates how considering bias shift after disturbance can reduce equifinality. Compared to 10^4 alternative sub-ensembles of eight parameter sets each randomly selected from the 30-member ensemble, the stationary sub-ensemble has significantly reduced uncertainty in LAI (p < 0.01) and transmissivity (p < 0.02), calculated from the cumulative distribution function for the fractional uncertainty reduction of all 10^4 sub-ensembles. This uncertainty reduction associated with the stationary sub-ensemble is 72% larger for LAI and 285% larger for log-transformed transmissivity compared to the median uncertainty reduction of same-sized sub-ensembles selected randomly. The stationary sub-ensemble has mean 2011-era LAI between 1.9-2.8 m²/m², which is 74% less uncertainty compared to the full behavioral ensemble range of 0.9-4.1 m²/m² (Fig. 5). Analogously, the stationary sub-ensemble has 50% less uncertainty in log-transformed mean transmissivity despite order-of-

magnitude residual uncertainty (108-1378 m²/d). Meteorological uncertainty remains mostly unchanged in the stationary subensemble, with 3.7 °C and 15% uncertainties in temperature and precipitation biases, respectively, compared to 4.4 °C and 15% for the behavioral ensemble (no significant change relative to random sub-ensemble selection). This leads to similar uncertainty in the stationary sub-ensemble's post-fire evaporative index (ET / P) compared to the full ensemble (25-34% vs. 24-39% respectively). Among all 14 calibrated parameters (Table 1), only the melt-season albedo decay rate has a statistically significant difference in the mean (p < 0.05, Welch two-sample t-test) between the stationary sub-ensemble and the full 30-member ensemble. Instead, most of the equifinality reduction arises from shrinking the uncertainty of the parameter distributions rather than changing their mean (Supplemental Fig. S4) and/or from constraining multi-dimensional parameter interactions (Supplemental Fig. S1). The 30-member behavioral ensemble has residual meteorological uncertainty ranging from -11% to +4% precipitation biases and -3.4 °C to +1.0 °C temperature biases. Considering only the 8-member stationary sub-ensemble, the precipitation bias uncertainty remains the same (-11% to +4%) and the temperature bias uncertainty decreases slightly to a range of -3.1 °C to +0.3 °C. Although these calibrated meteorological biases are substantially smaller than our ±25% calibration range (Table 1), the precipitation uncertainty remains roughly the same magnitude as the post-fire streamflow change, highlighting the potential confounding impact of forcing data on post-disturbance change-detection studies.

Compared to the full behavioral ensemble, the stationary sub-ensemble has slightly sub-optimal hydrograph fit (NSE 0.80-0.85 vs. 0.89 max), but better SWE volume error compared to the highest-NSE parameter set (MAPE of 18-27% across 30 ASO surveys vs. 32% for the highest-NSE parameter set). The stationary sub-ensemble has statistically lower (worse) mean NSE values compared to the 30-member ensemble (p < 0.05) and approaches the threshold for significantly lower (better) mean SWE volume percent error (p = 0.055). The >95th-percentile peak flow RMSE is also significantly worse (p < 0.05) for the stationary sub-ensemble. Differences in log-scale NSE and annual or April-July water yield error are not statistically significant. The improvement in snow skill despite a slight worsening of streamflow skill (Supplemental Fig. S5) may arise from overfitting during calibration, which leads to a tradeoff between enhanced model physical fidelity (represented by the near-zero bias shift and better snow performance of the stationary sub-ensemble) and minor degradation in the streamflow performance metrics.

Empirical regression and process-based simulations both suggest an increase in streamflow after the Creek Fire, albeit with different uncertainty ranges (Fig. 6). An empirical model (Eq. 3) fit to pre-fire data predicts relatively less post-fire streamflow than observed, implying a total streamflow increase of +12% with a 90% credible interval of +5 to +18% assuming that each year's error distribution is independent. (The 90% credible interval represents the 5^{th} -95th percentiles.) Although the four-year total streamflow increase is significant at p < 0.01, for individual post-fire years we cannot reject the null hypothesis (no change after disturbance) at the p < 0.01 level, and we cannot even reject the no-change hypothesis at the p < 0.1 level in 2021 or 2024. Compared to the pure statistical model based on the same meteorological data, our process-based modeling approach

yields remarkably similar uncertainty. All 30 behavioral DHSVM parameter sets indicate at least some streamflow increase in each post-fire year, with a similar mean increase of +12% and a marginally wider 90% range of +3 to +17% across the ensemble. Although the 90% uncertainty ranges are similar between DHSVM and the empirical regression, all of the DHSVM parameter sets show at least some increase. Additionally, within individual years, the DHSVM uncertainty can be much lower (e.g., in 2023, the DHSVM 90% range is +2 to +11%, while the empirical regression 90% credible interval is +3% to +23%). The uncertainty of the empirical model benefits from considering all four years simultaneously because the empirical model assumes that each year's fire effect is independent, while different DHSVM parameter sets are systematically biased high or low across all post-fire years.

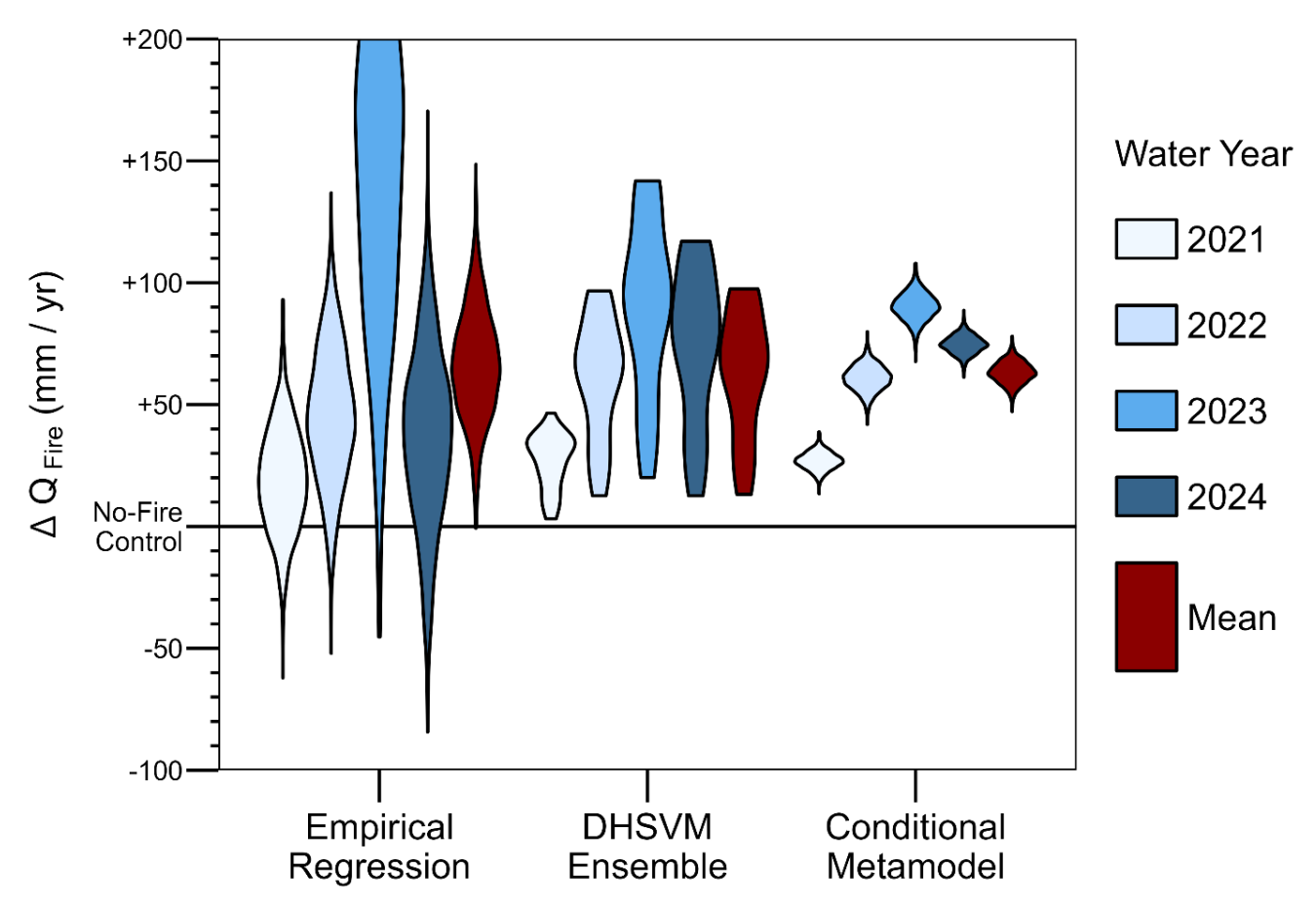


Figure 6: Uncertainty distributions for the annual post-fire streamflow change relative to a control scenario with no fire. Empirical regression results are estimated by comparing post-fire measurements with 1,000 random samples of a pre-fire multi-linear regression model (Eq. 3). The DHSVM ensemble represents the difference between fire-aware and no-fire control simulations using 30 different calibrated parameter sets. The conditional metamodel predicts the DHSVM response subject to the requirement of stationary bias using 1,000 random samples of the Bayesian regression in Eq. (2). (Note that the vertical axis is truncated at +200 mm/yr for increased visibility of most results.)

Compared to pure statistical or pure process-based approaches, a statistical metamodel trained on DHSVM results and conditioned on bias stationarity can drastically reduce uncertainty. Using 1,000 random samples of the metamodel (Eq. 2), we find a +11% increase in total post-fire streamflow with a 90% credible interval of +10 to +12%. The mean streamflow response is 14 standard deviations above zero, confidently rejecting the no-change hypothesis. Moreover, interannual variability in the conditional streamflow response is separable between all pairs of years at the p < 0.01 level. In contrast, raw DHSVM simulations of the streamflow response in 2022, 2023, and 2024 are not mutually separable at the p < 0.05 level. Comparing 90% credible intervals, the conditional approach reduces uncertainty in the total post-fire streamflow change by 80% compared to the empirical regression and 82% compared to the behavioral DHSVM ensemble. Of course we cannot know precisely what the true streamflow would have been without a fire, so some uncertainty must always remain, but our metamodel results suggest that we can substantially reduce this uncertainty by fusing process-based and statistical approaches.

The independent pre-fire calibration (end of Sect. 2.2) yields similar predictions of the post-fire streamflow change (Supplemental Figure S7). When applied to behavioral parameter sets from the pre-fire calibration, the conditional metamodel predicts a 90% credible interval of +9% to +12% for the total post-fire streamflow change, which is remarkably close to the independent estimate of +10% to +12% using the cross-fire (2015-2024) calibration. The conditional metamodel based on the pre-fire calibration reduces uncertainty in the total post-fire streamflow (90% confidence interval) by 82% compared to the empirical regression and 74% compared to the pre-fire behavioral DHSVM ensemble, which is again similar to the analogous 80% and 82% reductions (respectively) achieved by the cross-fire calibration metamodel. Regardless of whether DHSVM is calibrated pre- and post-fire, or only pre-fire, the conditional metamodel provides consistent predictions of the additional streamflow attributable to the Creek Fire (ΔQ_{Fire}).

4 Discussion

Hydrological models must includeaccount for forest fires and other environmental disturbances to provide robust predictions for water resource management, risk assessment, and operational planning. In 2021, the first year after the Creek Fire, our hybrid modeling approach estimates that the additional streamflow attributable to forest disturbance provided $0.11 \pm 0.03 \text{ km}^3$ (92,000 ac-ft.) of extra water to Millerton Lake (a major regional reservoir, Fig. 2), which is $18\% \pm 4\%$ of the total water yield in a year where drought conditions caused curtailment of downstream water rights (California DWR 2021). In the wet 2023 water year, extra streamflow attributable to the fire totaled $\sim 0.38 \pm 0.04 \text{ km}^3$ (310,000 ac-ft., 7% of total water yield), equivalent to an extra $60\% \pm 7\%$ of the reservoir storage capacity in a year with widespread flooding (California DWR 2023). (All uncertainty ranges indicate the 90% credible interval.) These examples illustrate the potential for landscape-scale forest disturbance to enhance water resources and/or exacerbate water risks (e.g., Boardman et al., 2025). Accurately representing disturbance and accounting for other sources of nonstationarity should be a priority of ecohydrological modeling.

Our results suggest that equifinality demands more thoughtful consideration in hydrological model-based studies of disturbance. At the same time, studies investigating disturbance have a unique and underutilized opportunity to reduce model equifinality. Much of the spread in the DHSVM ensemble (Fig. 6) could be eliminated by reducing the number of calibrated parameters or narrowing their prior range (Table 1). However, in typical landscape-scale simulations, we do not know the "correct" parameter values. For example, there is considerable uncertainty in vegetation properties derived from satellite imagery (Garrigues et al. 2008, Tang et al. 2019) or extrapolated from sparse field data (Meyer et al. 2016). Moreover, in modeling applications, "effective" parameters may subsume additional sources of structural or data uncertainty (Dolman and Blyth 1997, Vázquez 2003, Were et al. 2007), and some quasi-empirical parameters (e.g., grid-scale hydraulic conductivity) do not have single "correct" values (Beven 1993). In our current study, we choose to treat the combination of model and forcing data as a single inferential system, so uncertainty in hydrological parameters is not independent from meteorological biases. This unified approach is useful for our goal of simultaneously constraining multiple sources of uncertainty in the postfire streamflow change, but other studies may choose to use the same meteorological assumptions across all models to more tightly constrain and explore within-model dynamics. Uncertainty in vegetation properties like LAI can produce significantly different streamflow predictions (e.g., Bart et al. 2016 and Fig. 5 of this study), and latent uncertainty could cause systematic biases (Fig. 4). Furthermore, even if vegetation properties could be tightly constrained, introducing parameter variability into model experiments can reveal compensating ecohydrological processes (Figs. 1, 4), counterintuitively leading to higher confidence in the statistical metamodel by providing datapoints for regression in Eq. (2). Nevertheless, reducing model parameter uncertainty is generally desirable when justified, and our results show that a sub-ensemble of parameter sets with near-stationary bias after disturbance can significantly reduce uncertainty in LAI (p < 0.01) and transmissivity (p < 0.02).

560

565

570

575

580

585

590

Using process-based models for post-disturbance predictions based on traditional streamflow calibration metrics can be dangerously misleading. Describing model performance with simple goodness-of-fit metrics (e.g., NSE) is problematic in general due to sampling uncertainty and other issues (Clark et al. 2021), but these metrics remain ubiquitous in modeling studies (including this one) due to their ease of application and simplicity of interpretation. Although these metrics are useful for loosely identifying an initial ensemble of behavioral models, our results provide a clear example of the pitfalls in blindly trusting NSE-based (or similar) calibration strategies. In particular, the four models with the highest daily NSE (0.88-0.89) have anomalously small disturbance effects, and the parameter set with the absolute highest NSE underestimates the post-fire streamflow change by 79% relative to the metamodel mean (Supplemental Fig. S6). These outlying parameter sets are presumably compensating for unknown deficiencies in the model structure and/or forcing data, leading the model to get a slightly higher NSE for what are apparently the wrong reasons. These undesirable and yet numerically optimal solutions are endemic to high-dimensional optimization problems, an issue known as "reward hacking" (Amodei et al. 2016). Although log-transformed NSE appears less vulnerable to reward hacking (Supplemental Fig. S6), the parameter set with the absolute highest log NSE still underestimates the metamodel-based mean streamflow change by 58%. It is noteworthy that our ultimate model

evaluation metric (bias shift, Fig. 5) is not included in the calibration. If this metric were directly calibrated, it might be susceptible to reward hacking, leading to unreliable inference in Eq. (2).

595

600

605

610

With care, process-based models can remain powerful tools for hydrological investigation. Despite a recent focus on machine learning approaches to hydrological prediction (Ardabili et al. 2020, Xu and Liang 2021), purely empirical methods are limited by the amount of available data, the ability to assign clear process attribution, and the potentially ambiguous interpretation of nonstationarity (Slater et al. 2021). In the years immediately after a large forest disturbance (e.g., megafire), water managers may require rapid estimates of the potential hydrological impacts without the luxury of waiting for more data to accrue. Counterfactual model simulations can help isolate disturbance effects from stochastic weather and other variability, but it is notoriously challenging to quantify the uncertainty of distributed process-based models. Direct uncertainty estimation based on subjective likelihood metrics (e.g., GLUE, Beven and Binley 1992) is statistically unjustified (Mantovan and Todini 2006, Stedinger et al. 2008). Nevertheless, by using a subjective sample of models to constrain sensitivity (Fig. 5), we can perform classical Bayesian inference (Eq. 2) to sample the relationship between an unknown outcome (e.g., the streamflow response to fire) and an observational constraint (e.g., bias stationarity). This framework overcomes the statistical limitations of processbased models by treating the results from equifinal parameter sets as independent data points that constrain a statistical metamodel (Eq. 2), which should be transferable to other disturbance studies. Moreover, the statistical metamodel provides an 82% uncertainty reduction compared to the raw DHSVM ensemble with just four years of post-fire streamflow data in a single watershed. The consistency of the metamodel results between two independent calibrations (pre-fire and cross-fire) suggests that our framework is robust to subjective calibration decisions and random temporal variability, strengthening confidence in the results. Further calibration tests in other watersheds could inform a transferrable understanding of equifinality that might help constrain the post-fire streamflow response with fewer years of post-fire data, and could even help constrain predictions for possible future disturbances before they happen.

615

620

Our findings suggest a generally applicable conceptual framework for hydrological model simulations of many types of change beyond just environmental disturbance. In brief, it is important to ensure that our models are stationary with respect to the variability they are used to investigate. For our present study of the streamflow response to a forest fire, the model should have stationary bias across pre- and post-fire periods. For a study on climate warming effects, modelers could test the stationarity of model biases in warmer or cooler years or locations. For a drought study, model bias stationarity could be evaluated between wet and dry periods. Many analogous examples are easily imagined. We anticipate that testing bias stationarity across different types of change can help reduce both equifinality and uncertainty, as shown here.

5 Conclusion

630

635

640

645

650

In light of our results from this test application, we offer some general recommendations for process-based simulations of environmental disturbance in a hydrological context.

- Parameter uncertainty extends beyond the subsurface. We suggest calibrating or at least testing the sensitivity of parameters controlling the partitioning of ET fluxes (e.g., overstory/understory transpiration, interception loss, soil evaporation, etc.). Parameter interactions with meteorological uncertainty should also be considered and potentially propagated during calibration, especially when high-precision basin-scale forcing data are unavailable.
- Nonstationary error metrics (e.g., positive or negative bias shift) can indicate a failure to adequately represent change. Rejecting parameter sets with a bias shift after forest disturbance (or with respect to some other change) can help reduce equifinality and thus also reduce uncertainty in modeled hydrological responses to disturbance.
- Modelers should beware of "reward hacking" (i.e., overfitting) during calibration, particularly when applying powerful optimization algorithms to high-dimensional search spaces. In this study, selecting the highest-NSE parameter sets would lead to a 79% underestimation of the streamflow response to disturbance relative to the mean value of the conditional metamodel (analogous 58% underestimation using the highest log NSE).
- We caution against direct derivation of uncertainty ranges from subjective parameter ensembles, as this could lead to unnecessarily high uncertainty with poor statistical justification (Fig. 5). Instead, model results can inform a statistical metamodel conditioned on observation-based metrics related to stationarity (e.g., bias shift), enabling the derivation of uncertainty from conditional statistics (Eq. 2). The statistical metamodel structure will necessarily depend on the study objectives, but the principle is generally applicable to other models and types of environmental change.

Data and Code Availability

A Zenodo archive (Boardman 2025) includes all data, model code, and processing scripts needed to understand the study and recreate the figures (https://doi.org/10.5281/zenodo.16972670). In particular, the R script "5_BayesianModeling.R" and the Stan code "Bayesian_DHSVMbias.stan" may be useful for anyone interested in adapting our Bayesian conditional metamodel (Eq. 2) to other projects. SWE maps from Airborne Observatories, Inc., used for calibration are publicly available at https://data.airbornesnowobservatories.com/ (Airborne Snow Observatories, Inc., 2025).

Author Contribution

ENB and AAH formulated the project conceptualization. ENB developed the methodology and lead data curation, software development, visualization, and writing. GFSB contributed to methodology, visualization, and writing. MSW contributed to methodology and writing. RKS contributed to visualization and writing. AAH contributed to supervision, methodology, visualization, and writing.

Competing Interests

The authors declare that they have no conflict of interest relevant to this manuscript.

Financial Support

E. N. Boardman was partially supported by the NSF Graduate Research Fellowship Program under Grant #1937966. G. F. S. Boisrame was partially supported by NSF EAR #2011346 and NSF Grant No. OIA-2148788. A. A. Harpold was partially supported by NSF EAR #2012310.

References

- Abatzoglou, J. T.: Development of gridded surface meteorological data for ecological applications and modelling, International Journal of Climatology, 33, 121–131, https://doi.org/10.1002/joc.3413, 2013.
 - Abolafia-Rosenzweig, R., Gochis, D., Schwarz, A., Painter, T. H., Deems, J., Dugger, A., Casali, M., and He, C.: Quantifying the Impacts of Fire-Related Perturbations in WRF-Hydro Terrestrial Water Budget Simulations in California's Feather River Basin, Hydrological Processes, 38, e15314, https://doi.org/10.1002/hyp.15314, 2024.
- Airborne Snow Observatories, Inc.: Data Portal, https://data.airbornesnowobservatories.com/ (last access: 27 August 2025), 2025.
 - Amodei, D., Olah, C., Steinhardt, J., Christiano, P., Schulman, J., and Mané, D.: Concrete Problems in AI Safety, https://doi.org/10.48550/arXiv.1606.06565, 25 July 2016.
- Ardabili, S., Mosavi, A., Dehghani, M., and Várkonyi-Kóczy, A. R.: Deep Learning and Machine Learning in Hydrological Processes Climate Change and Earth Systems a Systematic Review, in: Engineering for Sustainable Future, Cham, 52–62, https://doi.org/10.1007/978-3-030-36841-8 5, 2020.
 - Ayars, J., Kramer, H. A., and Jones, G. M.: The 2020 to 2021 California megafires and their impacts on wildlife habitat, Proc. Natl. Acad. Sci. U.S.A., 120, e2312909120, https://doi.org/10.1073/pnas.2312909120, 2023.

- Bart, R. R.: A regional estimate of postfire streamflow change in California, Water Resources Research, 52, 1465–1478, https://doi.org/10.1002/2014WR016553, 2016.
 - Bart, R. R., Tague, C. L., and Moritz, M. A.: Effect of Tree-to-Shrub Type Conversion in Lower Montane Forests of the Sierra Nevada (USA) on Streamflow, PLOS ONE, 11, e0161805, https://doi.org/10.1371/journal.pone.0161805, 2016.
 - Bennett, A., Hamman, J., and Nijssen, B.: MetSim: A Python package for estimation and disaggregation of meteorological data, JOSS, 5, 2042, https://doi.org/10.21105/joss.02042, 2020.
- Beven, K.: Prophecy, reality and uncertainty in distributed hydrological modelling, Advances in Water Resources, 16, 41–51, https://doi.org/10.1016/0309-1708(93)90028-E, 1993.
 - Beven, K.: A manifesto for the equifinality thesis, Journal of Hydrology, 320, 18–36, https://doi.org/10.1016/j.jhydrol.2005.07.007, 2006.
 - Beven, K. and Binley, A.: The future of distributed models: Model calibration and uncertainty prediction, Hydrological Processes, 6, 279–298, https://doi.org/10.1002/hyp.3360060305, 1992.

- Bieger, K., Rathjens, H., Allen, P. M., and Arnold, J. G.: Development and Evaluation of Bankfull Hydraulic Geometry Relationships for the Physiographic Regions of the United States, JAWRA Journal of the American Water Resources Association, 51, 842–858, https://doi.org/10.1111/jawr.12282, 2015.
- Binois, M. and Picheny, V.: **GPareto**: An *R* Package for Gaussian-Process-Based Multi-Objective Optimization and Analysis, J. Stat. Soft., 89, https://doi.org/10.18637/jss.v089.i08, 2019.
 - Birkel, C., Arciniega-Esparza, S., Maneta, M. P., Boll, J., Stevenson, J. L., Benegas-Negri, L., Tetzlaff, D., and Soulsby, C.: Importance of measured transpiration fluxes for modelled ecohydrological partitioning in a tropical agroforestry system, Agricultural and Forest Meteorology, 346, 109870, https://doi.org/10.1016/j.agrformet.2023.109870, 2024.
- Boardman, E.: Data and Code for Megafire Disturbance Hydrological Model Calibration Study, Zenodo [data set], https://doi.org/10.5281/zenodo.16972670, 2025.
 - Boardman, E. N., Renshaw, C. E., Shriver, R. K., Walters, R., McGurk, B., Painter, T. H., Deems, J. S., Bormann, K. J., Lewis, G. M., Dethier, E. N., and Harpold, A. A.: Sources of seasonal water supply forecast uncertainty during snow drought in the Sierra Nevada, J American Water Resour Assoc, 60, 972–990, https://doi.org/10.1111/1752-1688.13221, 2024.
- Boardman, E. N., Duan, Z., Wigmosta, M. S., Flake, S. W., Sloggy, M. R., Tarricone, J., and Harpold, A. A.: Restoring Historic Forest Disturbance Frequency Would Partially Mitigate Droughts in the Central Sierra Nevada Mountains, Water Resources Research, 61, e2024WR039227, https://doi.org/10.1029/2024WR039227, 2025.
 - Boisramé, G. F. S., Thompson, S. E., Tague, C. (Naomi), and Stephens, S. L.: Restoring a Natural Fire Regime Alters the Water Balance of a Sierra Nevada Catchment, Water Resources Research, 55, 5751–5769, https://doi.org/10.1029/2018WR024098, 2019.
- Preiman, L., Cutler, A., Liaw, A., and Wiener, M.: randomForest: Breiman and Cutlers Random Forests for Classification and Regression, https://doi.org/10.32614/CRAN.package.randomForest, 2002.

- Buma, B.: Disturbance interactions: characterization, prediction, and the potential for cascading effects, Ecosphere, 6, art70, https://doi.org/10.1890/ES15-00058.1, 2015.
- California DWR: Water Year 2021: An Extreme Year, https://water.ca.gov/-/media/DWR-Website/Web-Pages/Water-715
 https://water.ca.gov/-/media/DWR-Website/Web-Pages/Water-715
 https://water.ca.gov/-/media/DWR-Website/Web-Pages/Water-715
 https://water-Year-2021-broch_v2.pdf
 (last access: 4 February 2025), 2021.
 - California DWR: Water Year 2023: Weather Whiplash, From Drought To Deluge, https://water.ca.gov/-/media/DWR-Website/Web-Pages/Water-Basics/Drought/Files/Publications-And-Reports/Water-Year-2023-wrap-up-brochure_01.pdf (last access: 4 February 2025), 2023.
- 720 California DWR: Database of full natural flow records for the SBF station, https://cdec.water.ca.gov/dynamicapp/staMeta?station_id=SBF (last access: 27 August 2025), 2024,
 - Clark, M. P., Vogel, R. M., Lamontagne, J. R., Mizukami, N., Knoben, W. J. M., Tang, G., Gharari, S., Freer, J. E., Whitfield, P. H., Shook, K. R., and Papalexiou, S. M.: The Abuse of Popular Performance Metrics in Hydrologic Modeling, Water Resources Research, 57, e2020WR029001, https://doi.org/10.1029/2020WR029001, 2021.
- Cuo, L., Giambelluca, T. W., and Ziegler, A. D.: Lumped parameter sensitivity analysis of a distributed hydrological model within tropical and temperate catchments, Hydrological Processes, 25, 2405–2421, https://doi.org/10.1002/hyp.8017, 2011.
 - Dewitz, J. and U.S. Geological Survey: National Land Cover Database (NLCD) 2019 Products, https://doi.org/10.5066/P9JZ7AO3, 2019.
- 730 Dolman, A. J. and Blyth, E. M.: Patch scale aggregation of heterogeneous land surface cover for mesoscale meteorological models, Journal of Hydrology, 190, 252–268, https://doi.org/10.1016/S0022-1694(96)03129-0, 1997.
 - Du, E., Link, T. E., Gravelle, J. A., and Hubbart, J. A.: Validation and sensitivity test of the distributed hydrology soil-vegetation model (DHSVM) in a forested mountain watershed, Hydrol. Process., 28, 6196–6210, https://doi.org/10.1002/hyp.10110, 2014.
- Dupuy, D., Helbert, C., and Franco, J.: DiceDesign and DiceEval: Two R Packages for Design and Analysis of Computer Experiments, Journal of Statistical Software, 65, 1–38, https://doi.org/10.18637/jss.v065.i11, 2015.
 - Ebel, B. A. and Loague, K.: Physics-based hydrologic-response simulation: Seeing through the fog of equifinality, Hydrological Processes, 20, 2887–2900, https://doi.org/10.1002/hyp.6388, 2006.
- Ebel, B. A. and Mirus, B. B.: Disturbance hydrology: challenges and opportunities, Hydrological Processes, 28, 5140–5148, https://doi.org/10.1002/hyp.10256, 2014.
 - Eidenshink, J., Schwind, B., Brewer, K., Zhu, Z.-L., Quayle, B., and Howard, S.: A Project for Monitoring Trends in Burn Severity, fire ecol, 3, 3–21, https://doi.org/10.4996/fireecology.0301003, 2007.
 - Elsner, M. M., Gangopadhyay, S., Pruitt, T., Brekke, L. D., Mizukami, N., and Clark, M. P.: How Does the Choice of Distributed Meteorological Data Affect Hydrologic Model Calibration and Streamflow Simulations?, Journal of Hydrometeorology, 15, 1384–1403, https://doi.org/10.1175/JHM-D-13-083.1, 2014.

- Emmerich, M. T. M., Deutz, A. H., and Klinkenberg, J. W.: Hypervolume-based expected improvement: Monotonicity properties and exact computation, in: 2011 IEEE Congress of Evolutionary Computation (CEC), 2011 IEEE Congress of Evolutionary Computation (CEC), 2147–2154, https://doi.org/10.1109/CEC.2011.5949880, 2011.
- Fan, Y. and Miguez-Macho, G.: A simple hydrologic framework for simulating wetlands in climate and earth system models, Clim Dyn, 37, 253–278, https://doi.org/10.1007/s00382-010-0829-8, 2011.

- Fatichi, S., Vivoni, E. R., Ogden, F. L., Ivanov, V. Y., Mirus, B., Gochis, D., Downer, C. W., Camporese, M., Davison, J. H., Ebel, B., Jones, N., Kim, J., Mascaro, G., Niswonger, R., Restrepo, P., Rigon, R., Shen, C., Sulis, M., and Tarboton, D.: An overview of current applications, challenges, and future trends in distributed process-based models in hydrology, Journal of Hydrology, 537, 45–60, https://doi.org/10.1016/j.jhydrol.2016.03.026, 2016.
- Fisher, R. A. and Koven, C. D.: Perspectives on the Future of Land Surface Models and the Challenges of Representing Complex Terrestrial Systems, Journal of Advances in Modeling Earth Systems, 12, e2018MS001453, https://doi.org/10.1029/2018MS001453, 2020.
 - Franks, S. W., Beven, K. J., Quinn, P. F., and Wright, I. R.: On the sensitivity of soil-vegetation-atmosphere transfer (SVAT) schemes: equifinality and the problem of robust calibration, Agricultural and Forest Meteorology, 86, 63–75, https://doi.org/10.1016/S0168-1923(96)02421-5, 1997.
 - Furniss, T. J., Povak, N. A., Hessburg, P. F., Salter, R. B., Duan, Z., and Wigmosta, M.: Informing climate adaptation strategies using ecological simulation models and spatial decision support tools, Front. For. Glob. Change, 6, https://doi.org/10.3389/ffgc.2023.1269081, 2023.
- Garrigues, S., Lacaze, R., Baret, F., Morisette, J. T., Weiss, M., Nickeson, J. E., Fernandes, R., Plummer, S., Shabanov, N. V.,
 Myneni, R. B., Knyazikhin, Y., and Yang, W.: Validation and intercomparison of global Leaf Area Index products derived from remote sensing data, Journal of Geophysical Research: Biogeosciences, 113, https://doi.org/10.1029/2007JG000635,
 2008.
 - Goeking, S. A. and Tarboton, D. G.: Forests and Water Yield: A Synthesis of Disturbance Effects on Streamflow and Snowpack in Western Coniferous Forests, Journal of Forestry, 118, 172–192, https://doi.org/10.1093/jofore/fvz069, 2020.
- Goeking, S. A. and Tarboton, D. G.: Spatially Distributed Overstory and Understory Leaf Area Index Estimated from Forest Inventory Data, Water, 14, 2414, https://doi.org/10.3390/w14152414, 2022a.
 - Goeking, S. A. and Tarboton, D. G.: Variable Streamflow Response to Forest Disturbance in the Western US: A Large-Sample Hydrology Approach, Water Resources Research, 58, e2021WR031575, https://doi.org/10.1029/2021WR031575, 2022b.
 - Goodhart, C.: Problems of Monetary Management: The U.K. Experience, Springer, 1984.
- 775 Grayson, R. B., Moore, I. D., and McMahon, T. A.: Physically based hydrologic modeling: 1. A terrain-based model for investigative purposes, Water Resources Research, 28, 2639–2658, https://doi.org/10.1029/92WR01258, 1992.
 - Gupta, S., Papritz, A., Lehmann, P., Hengl, T., Bonetti, S., and Or, D.: Global Mapping of Soil Water Characteristics Parameters— Fusing Curated Data with Machine Learning and Environmental Covariates, Remote Sensing, 14, 1947, https://doi.org/10.3390/rs14081947, 2022.

- Hampton, T. B. and Basu, N. B.: A novel Budyko-based approach to quantify post-forest-fire streamflow response and recovery timescales, Journal of Hydrology, 608, 127685, https://doi.org/10.1016/j.jhydrol.2022.127685, 2022.
 - Henn, B., Newman, A. J., Livneh, B., Daly, C., and Lundquist, J. D.: An assessment of differences in gridded precipitation datasets in complex terrain, Journal of Hydrology, 556, 1205–1219, https://doi.org/10.1016/j.jhydrol.2017.03.008, 2018.
 - Her, Y. and Chaubey, I.: Impact of the numbers of observations and calibration parameters on equifinality, model performance, and output and parameter uncertainty: Parameters, Observations, and Uncertainty, Hydrol. Process., 29, 4220–4237, https://doi.org/10.1002/hyp.10487, 2015.

790

795

800

- Hirsch, R. M.: A Perspective on Nonstationarity and Water Management, JAWRA Journal of the American Water Resources Association, 47, 436–446, https://doi.org/10.1111/j.1752-1688.2011.00539.x, 2011.
- Huang, G. and Kadir, T.: Estimates of Natural and Unimpaired Flows for the Central Valley of California: Water Years 1922-2014, Department of Water Resources, Bay-Delta Office, 2016.
- Huang, X. and Swain, D. L.: Climate change is increasing the risk of a California megaflood, Science Advances, 8, eabq0995, https://doi.org/10.1126/sciadv.abq0995, 2022.
- Johnson, R. S. H. and Alila, Y.: Nonstationary stochastic paired watershed approach: Investigating forest harvesting effects on floods in two large, nested, and snow-dominated watersheds in British Columbia, Canada, Journal of Hydrology, 625, 129970, https://doi.org/10.1016/j.jhydrol.2023.129970, 2023.
- Johnstone, J. F., Allen, C. D., Franklin, J. F., Frelich, L. E., Harvey, B. J., Higuera, P. E., Mack, M. C., Meentemeyer, R. K., Metz, M. R., Perry, G. L., Schoennagel, T., and Turner, M. G.: Changing disturbance regimes, ecological memory, and forest resilience, Frontiers in Ecology and the Environment, 14, 369–378, https://doi.org/10.1002/fee.1311, 2016.
- Jones, D. R., Schonlau, M., and Welch, W. J.: Efficient Global Optimization of Expensive Black-Box Functions, Journal of Global Optimization, 13, 455–492, https://doi.org/10.1023/A:1008306431147, 1998.
- Kang, T.-H. and Sharma, A.: A state-controlled hypothesis test for paired-watershed experiments, Journal of Hydrology, 640, 131664, https://doi.org/10.1016/j.jhydrol.2024.131664, 2024.
- Kavetski, D., Franks, S. W., and Kuczera, G.: Confronting input uncertainty in environmental modelling, in: Water Science and Application, vol. 6, edited by: Duan, Q., Gupta, H. V., Sorooshian, S., Rousseau, A. N., and Turcotte, R., American Geophysical Union, Washington, D. C., 49–68, https://doi.org/10.1029/WS006p0049, 2003.
- Kelleher, C., McGlynn, B., and Wagener, T.: Characterizing and reducing equifinality by constraining a distributed catchment model with regional signatures, local observations, and process understanding, Hydrology and Earth System Sciences, 21, 3325–3352, https://doi.org/10.5194/hess-21-3325-2017, 2017.
- Kennedy, J. and Eberhart, R.: Particle swarm optimization, in: Proceedings of ICNN'95 International Conference on Neural
 Networks, Proceedings of ICNN'95 International Conference on Neural Networks, 1942–1948 vol.4, https://doi.org/10.1109/ICNN.1995.488968, 1995.

- Khatami, S., Peel, M. C., Peterson, T. J., and Western, A. W.: Equifinality and Flux Mapping: A New Approach to Model Evaluation and Process Representation Under Uncertainty, Water Resources Research, 55, 8922–8941, https://doi.org/10.1029/2018WR023750, 2019.
- 815 LANDFIRE: LANDFIRE 2022 Existing Vegetation Type (EVT), 2022.

- Lundquist, J. D., Abel, M. R., Henn, B., Gutmann, E. D., Livneh, B., Dozier, J., and Neiman, P.: High-Elevation Precipitation Patterns: Using Snow Measurements to Assess Daily Gridded Datasets across the Sierra Nevada, California, Journal of Hydrometeorology, 16, 1773–1792, https://doi.org/10.1175/JHM-D-15-0019.1, 2015.
- Manning, A. L., Harpold, A., and Csank, A.: Spruce Beetle Outbreak Increases Streamflow From Snow-Dominated Basins in Southwest Colorado, USA, Water Resources Research, 58, e2021WR029964, https://doi.org/10.1029/2021WR029964, 2022.
 - Mantovan, P. and Todini, E.: Hydrological forecasting uncertainty assessment: Incoherence of the GLUE methodology, Journal of Hydrology, 330, 368–381, https://doi.org/10.1016/j.jhydrol.2006.04.046, 2006.
- Marshall, A. M., Abatzoglou, J. T., Rahimi, S., Lettenmaier, D. P., and Hall, A.: California's 2023 snow deluge:

 Contextualizing an extreme snow year against future climate change, Proceedings of the National Academy of Sciences,

 121, e2320600121, https://doi.org/10.1073/pnas.2320600121, 2024.
 - Meili, N., Beringer, J., Zhao, J., and Fatichi, S.: Aerodynamic effects cause higher forest evapotranspiration and water yield reductions after wildfires in tall forests, Global Change Biology, 30, e16995, https://doi.org/10.1111/gcb.16995, 2024.
 - Melsen, L. A., Addor, N., Mizukami, N., Newman, A. J., Torfs, P. J. J. F., Clark, M. P., Uijlenhoet, R., and Teuling, A. J.: Mapping (dis)agreement in hydrologic projections, Hydrol. Earth Syst. Sci., 22, 1775–1791. https://doi.org/10.5194/hess-22-1775-2018, 2018.
 - Meyer, C., Weigelt, P., and Kreft, H.: Multidimensional biases, gaps and uncertainties in global plant occurrence information, Ecology Letters, 19, 992–1006, https://doi.org/10.1111/ele.12624, 2016.
- Milly, P. C. D., Betancourt, J., Falkenmark, M., Hirsch, R. M., Kundzewicz, Z. W., Lettenmaier, D. P., and Stouffer, R. J.: Stationarity Is Dead: Whither Water Management?, Science, 319, 573–574, https://doi.org/10.1126/science.1151915, 2008.
 - Milly, P. C. D., Betancourt, J., Falkenmark, M., Hirsch, R. M., Kundzewicz, Z. W., Lettenmaier, D. P., Stouffer, R. J., Dettinger, M. D., and Krysanova, V.: On Critiques of "Stationarity is Dead: Whither Water Management?," Water Resources Research, 51, 7785–7789, https://doi.org/10.1002/2015WR017408, 2015.
- Moreno, H. A., Gupta, H. V., White, D. D., and Sampson, D. A.: Modeling the distributed effects of forest thinning on the long-term water balance and streamflow extremes for a semi-arid basin in the southwestern US, Hydrology and Earth System Sciences, 20, 1241–1267, https://doi.org/10.5194/hess-20-1241-2016, 2016.
 - MTBS Project (USDA Forest Service / U.S. Geological Survey): MTBS Data Access: Fire Level Geospatial Data, 2022.

- Pagano, T., Garen, D., and Sorooshian, S.: Evaluation of Official Western U.S. Seasonal Water Supply Outlooks, 1922–2002,

 Journal of Hydrometeorology, 5, 896–909, <a href="https://doi.org/10.1175/1525-7541(2004)005<0896:EOOWUS>2.0.CO;2">https://doi.org/10.1175/1525-7541(2004)005<0896:EOOWUS>2.0.CO;2,
 2004.
 - Painter, T. H., Berisford, D. F., Boardman, J. W., Bormann, K. J., Deems, J. S., Gehrke, F., Hedrick, A., Joyce, M., Laidlaw, R., Marks, D., Mattmann, C., McGurk, B., Ramirez, P., Richardson, M., Skiles, S. M., Seidel, F. C., and Winstral, A.: The Airborne Snow Observatory: Fusion of scanning lidar, imaging spectrometer, and physically-based modeling for mapping snow water equivalent and snow albedo, Remote Sensing of Environment, 184, 139–152, https://doi.org/10.1016/j.rse.2016.06.018, 2016.

- Pomeroy, J. W., Gray, D. M., Hedstrom, N. R., and Janowicz, J. R.: Physically Based Estimation of Seasonal Snow Accumulation in the Boreal Forest, in: Proceedings of the 59th Eastern Snow Conference, 93–108, 2002.
- Pongratz, J., Dolman, H., Don, A., Erb, K.-H., Fuchs, R., Herold, M., Jones, C., Kuemmerle, T., Luyssaert, S., Meyfroidt, P., and Naudts, K.: Models meet data: Challenges and opportunities in implementing land management in Earth system models, Global Change Biology, 24, 1470–1487, https://doi.org/10.1111/gcb.13988, 2018.
 - Rigge, M., Homer, C., Shi, H., Meyer, D., Bunde, B., Granneman, B., Postma, K., Danielson, P., Case, A., and Xian, G.: Rangeland Fractional Components Across the Western United States from 1985 to 2018, Remote Sensing, 13, 813, https://doi.org/10.3390/rs13040813, 2021a.
- Rigge, M. B., Bunde, B., Shi, H., and Postma, K.: Rangeland Condition Monitoring Assessment and Projection (RCMAP)
 Fractional Component Time-Series Across the Western U.S. 1985-2020 (2.0, October 2021),
 https://doi.org/10.5066/P95IQ4BT, 2021b.
 - Roustant, O., Ginsbourger, D., and Deville, Y.: DiceKriging, DiceOptim: Two R Packages for the Analysis of Computer Experiments by Kriging-Based Metamodeling and Optimization, Journal of Statistical Software, 51, 1–55, https://doi.org/10.18637/jss.v051.i01, 2012.
 - Saksa, P. C., Conklin, M. H., Battles, J. J., Tague, C. L., and Bales, R. C.: Forest thinning impacts on the water balance of Sierra Nevada mixed-conifer headwater basins, Water Resources Research, 53, 5364–5381, https://doi.org/10.1002/2016WR019240, 2017.
- Salas, J. D., Rajagopalan, B., Saito, L., and Brown, C.: Special Section on Climate Change and Water Resources: Climate

 Nonstationarity and Water Resources Management, Journal of Water Resources Planning and Management, 138, 385–

 388, https://doi.org/10.1061/(ASCE)WR.1943-5452.0000279, 2012.
 - Schreiner-McGraw, A. P. and Ajami, H.: Combined impacts of uncertainty in precipitation and air temperature on simulated mountain system recharge from an integrated hydrologic model, Hydrology and Earth System Sciences, 26, 1145–1164, https://doi.org/10.5194/hess-26-1145-2022, 2022.
- Seibert, J., & McDonnell, J. J. Land-cover impacts on streamflow: a change-detection modelling approach that incorporates parameter uncertainty. Hydrological Sciences Journal, 55(3), 316–332. https://doi.org/10.1080/02626661003683264, 2010.

- Shields, C. A. and Tague, C. L.: Assessing the Role of Parameter and Input Uncertainty in Ecohydrologic Modeling:

 Implications for a Semi-arid and Urbanizing Coastal California Catchment, Ecosystems, 15, 775–791,

 https://doi.org/10.1007/s10021-012-9545-z, 2012.
 - Slater, L. J., Anderson, B., Buechel, M., Dadson, S., Han, S., Harrigan, S., Kelder, T., Kowal, K., Lees, T., Matthews, T., Murphy, C., and Wilby, R. L.: Nonstationary weather and water extremes: a review of methods for their detection, attribution, and management, Hydrology and Earth System Sciences, 25, 3897–3935, https://doi.org/10.5194/hess-25-3897-2021, 2021.
- 885 Soil Survey Staff: Soil Survey Geographic (SSURGO) Database, https://sdmdataaccess.sc.egov.usda.gov (last access: 27 August 2025), 2022.
 - Spear, R. C. and Hornberger, G. M.: Eutrophication in peel inlet—II. Identification of critical uncertainties via generalized sensitivity analysis, Water Research, 14, 43–49, https://doi.org/10.1016/0043-1354(80)90040-8, 1980.
 - Stan Development Team: Stan Modeling Language Users Guide and Reference Manual, 2.32.5, 2023.
- Stedinger, J. R., Vogel, R. M., Lee, S. U., and Batchelder, R.: Appraisal of the generalized likelihood uncertainty estimation (GLUE) method, Water Resources Research, 44, https://doi.org/10.1029/2008WR006822, 2008.
 - Stephens, S. L., Bernal, A. A., Collins, B. M., Finney, M. A., Lautenberger, C., and Saah, D.: Mass fire behavior created by extensive tree mortality and high tree density not predicted by operational fire behavior models in the southern Sierra Nevada, Forest Ecology and Management, 518, 120258, https://doi.org/10.1016/j.foreco.2022.120258, 2022.
- Sun, N., Yan, H., Wigmosta, M. S., Leung, L. R., Skaggs, R., and Hou, Z.: Regional Snow Parameters Estimation for Large-Domain Hydrological Applications in the Western United States, Journal of Geophysical Research: Atmospheres, 124, 5296–5313, https://doi.org/10.1029/2018JD030140, 2019.
 - Tague, C., Seaby, L., and Hope, A.: Modeling the eco-hydrologic response of a Mediterranean type ecosystem to the combined impacts of projected climate change and altered fire frequencies, Climatic Change, 93, 137–155, https://doi.org/10.1007/s10584-008-9497-7, 2009.
 - Tang, H., Song, X.-P., Zhao, F. A., Strahler, A. H., Schaaf, C. L., Goetz, S., Huang, C., Hansen, M. C., and Dubayah, R.: Definition and measurement of tree cover: A comparative analysis of field-, lidar- and landsat-based tree cover estimations in the Sierra national forests, USA, Agricultural and Forest Meteorology, 268, 258–268, https://doi.org/10.1016/j.agrformet.2019.01.024, 2019.
- 905 U.S. Geological Survey: USGS TNM Hydrography (NHD), 2019.

- Vázquez, R. F.: Effect of potential evapotranspiration estimates on effective parameters and performance of the MIKE SHE-code applied to a medium-size catchment, Journal of Hydrology, 270, 309–327, https://doi.org/10.1016/S0022-1694(02)00308-6, 2003.
- Vögeli, C., Lehning, M., Wever, N., and Bavay, M.: Scaling Precipitation Input to Spatially Distributed Hydrological Models by Measured Snow Distribution, Front. Earth Sci., 4, https://doi.org/10.3389/feart.2016.00108, 2016.

- Vrugt, J. A. and Beven, K. J.: Embracing equifinality with efficiency: Limits of Acceptability sampling using the DREAM(LOA) algorithm, Journal of Hydrology, 559, 954–971, https://doi.org/10.1016/j.jhydrol.2018.02.026, 2018.
- Were, A., Villagarcía, L., Domingo, F., Alados-Arboledas, L., and Puigdefábregas, J.: Analysis of effective resistance calculation methods and their effect on modelling evapotranspiration in two different patches of vegetation in semi-arid SE Spain, Hydrology and Earth System Sciences, 11, 1529–1542, https://doi.org/10.5194/hess-11-1529-2007, 2007.

920

925

- Wigmosta, M. S., Vail, L. W., and Lettenmaier, D. P.: A distributed hydrology-vegetation model for complex terrain, Water Resour. Res., 30, 1665–1679, https://doi.org/10.1029/94WR00436, 1994.
- Williams, A. P., Livneh, B., McKinnon, K. A., Hansen, W. D., Mankin, J. S., Cook, B. I., Smerdon, J. E., Varuolo-Clarke, A. M., Bjarke, N. R., Juang, C. S., and Lettenmaier, D. P.: Growing impact of wildfire on western US water supply, Proc. Natl. Acad. Sci. U.S.A., 119, e2114069119, https://doi.org/10.1073/pnas.2114069119, 2022.
- Winsemius, S., Babcock, C., Kane, V. R., Bormann, K. J., Safford, H. D., and Jin, Y.: Improved aboveground biomass estimation and regional assessment with aerial lidar in California's subalpine forests, Carbon Balance Manage, 19, 41, https://doi.org/10.1186/s13021-024-00286-w, 2024.
- Xu, T. and Liang, F.: Machine learning for hydrologic sciences: An introductory overview, WIREs Water, 8, e1533, https://doi.org/10.1002/wat2.1533, 2021.
 - Yang, Y., Roderick, M. L., Yang, D., Wang, Z., Ruan, F., McVicar, T. R., Zhang, S., and Beck, H. E.: Streamflow stationarity in a changing world, Environ. Res. Lett., 16, 064096, https://doi.org/10.1088/1748-9326/ac08c1, 2021.
 - Zambrano-Bigiarini, M., Rojas, and R.: A model-independent Particle Swarm Optimisation software for model calibration, Environmental Modelling & Software, 43, 5–25, https://doi.org/10.1016/j.envsoft.2013.01.004, 2013.
- 2009, 2009. Zehe, E. and Sivapalan, M.: Threshold behaviour in hydrological systems as (human) geo-ecosystems: manifestations, controls, implications, Hydrology and Earth System Sciences, 13, 1273–1297, https://doi.org/10.5194/hess-13-1273-2009, 2009.
 - Zolkos, S. G., Goetz, S. J., and Dubayah, R.: A meta-analysis of terrestrial aboveground biomass estimation using lidar remote sensing, Remote Sensing of Environment, 128, 289–298, https://doi.org/10.1016/j.rse.2012.10.017, 2013.